581
9-15-77

Lb. 1414

LBL-6332
UC-66b
TID-4500-R65

Energy and Environment Division

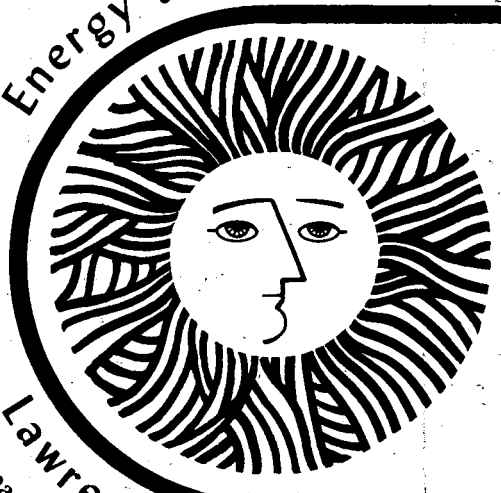

An Analysis of the Bipole-Dipole Resistivity Method for Geothermal Exploration

Abhijit Dey and H.F. Morrison

June 1977

Lawrence Berkeley Laboratory University of California/Berkeley

Prepared for the U.S. Energy Research and Development Administration under Contract No. W-7405-ENG-48

LBL-6332

Printed in the United States of America
Available from
National Technical Information Service
U. S. Department of Commerce
5285 Port Royal Road
Springfield, VA 22161
Price: Printed Copy ~~$4.50~~ 5.25 Microfiche $3.00

An Analysis of the Bipole-Dipole Resistivity Method for Geothermal Exploration

Abhijit Dey

H.F. Morrison

ABSTRACT

Bipole-dipole (B-D) resistivity mapping has been widely used as a reconnaissance method in geothermal exploration. In this technique, apparent resistivities are plotted at roving dipole receiver locations and the current source (bipole) is left fixed. Interpretation to date has been in terms of simple layered, dike, vertical contact, or sphere models. In the case of more complicated two-dimensional models the interpretation is much more ambiguous and the detection of buried conductors depends very much on the choice of transmitter location. Since apparent resistivities taken on a line collinear with the bipole are roughly equivalent to the apparent resistivities for one sounding in a dipole-dipole (D-D) pseudo-section, the two methods have been compared for several two-dimensional models.

A buried quarter space and a buried horizontal block of rectangular cross section, with or without an overburden layer, have been used in the comparison. Unless the target is very shallow or close to the bipole or dipole, the resolution of the horizontal position or depth extent for the B-D method is very poor. Conductive overburden worsens the situation for both methods but the effect is more drastic for the B-D method. The spatial patterns for these models is complex for the B-D method and in fact for certain transmitter positions only subtle differences exist for the buried block and buried quarter space models. Multiple sources improve the resolution of the B-D method, but many sources coupled with the high sampling density of receivers required to define the spatial patterns would greatly reduce the cost effectiveness claimed for this method. Changing the bipole orientation with respect to the strike of the models contributes little if anything to the resolution of the models. A further experiment of calculating a residual map by subtracting the half-space or layered half-space response from the response of the buried models was also unsuccessful in improving the interpretability of the B-D method. Finally, a model representative of a typical Basin-and-Range valley with and without a hypothesized geothermal reservoir shows that in more complex models the B-D map would not, in a practical survey, reveal the reservoir.

From these model studies it is clear that, except for some simple geologic situations, the B-D method is not effective for subsurface mapping. Selected D-D lines would be far more useful and more cost effective.

Introduction

Electrical resistivity distribution in the earth has been shown to be useful in the delineation of geothermal reservoirs. For the measurement of the electrical resistivity a pair of electrodes is used to inject a known d.c. current in the ground and the distribution of the d.c. potential or field is measured with a second pair in a surrounding area. Various combinations of the electrode deployment have been in use for purposes of sounding (determination of the vertical variation in resistivity assuming no lateral change) or profiling (determination of lateral changes in resistivity extending up to an assumed fixed depth of search).

In geothermal reservoir delineation work two different electrode configurations are commonly employed. One of these is the bipole-dipole mapping method and the other is the collinear dipole-dipole profiling method. In the collinear dipole-dipole configuration, first described by Hallof (1957), a transmitting dipole and a receiving dipole, each of equal length, a, are deployed in line with a dipole separation of Na. This configuration is illustrated in Figure 1a. The entire configuration is first moved along a survey line with a fixed dipole separation (N = constant), in a resistivity profiling mode. The traversing of the line with this configuration is then repeated with different values of N(=1, 2....10) thus providing successive resistivity profiles with progressively increasing depth of search. The resulting apparent resistivity data is plotted in the standard pseudo-section form, in between the transmitting and the receiving dipole. At the end of a survey along a line, this technique, therefore, yields a combination of both profiling and sounding mode data. the collinear dipole-dipole technique has found widespread application in mineral exploration, regional geologic mapping and detailed high resolution structural surveys. The response of this technique generally provides a high resolution of lateral variation in resistivity, good depth of search and relatively small effects from shallow, thin "geologic" noise sources. A

comparison of the response of this dipole-dipole method with those of the pole-dipole, Unipole and Schlumberger profiling arrays, over two dimensional resistivity structures, is shown by Dey, Meyer, Morrison and Dolan (1975). A similar analysis has been presented by Coggon (1971). A thorough comparison of the Schlumberger and dipole-dipole methods has been made by Beyer (1977).

In the bipole-dipole mapping configuration, the earth is energized by a pair of current electrodes fixed at a given location. The dimension of this transmitting dipole is usually large, of the order of 2-5 km,and the source dipole is called a "bipole." The electric fields or the potential differences between small receiver dipoles, usually oriented orthogonally, are then mapped in detail on the surface of the earth in a region surrounding the transmitting bipole. Variations in electric field behavior between adjacent receiver locations can be identified with changes in earth resistivity in the proximity of the receiver stations, rather than with earth properties at the source location or at points between the source and receiver (Keller, Furgerson, Lee, Harthill and Jacobson, 1975). This method is a variation of the equipotential survey technique described by Heiland (1940) and has recently been extensively used in geothermal reservoir exploration (e.g. Risk et al, 1970, Keller et al. 1975 , Stanley et al., 1976).

In the early applications of resistivity techniques to geothermal exploration, the bipole-dipole mapping method gained susbstantial prominence because of the rapidity and ease of operating procedures as a practical reconnaissance method. In large survey areas for geothermal exploration, it is logistically much more attractive to have a fixed transmitting bipole and a large number of roving orthogonal receiver dipoles. Many more current electrode preparations are required for collinear dipole surveys to cover the same areal extent. However, it soon became apparent that to define a zone of substantial changes in bulk apparent resistivity, several transmitters at different locations were required together with a rather high

density of observation points. In addition, all too often, the resulting maps are used for detailed interpretation of the resistivity structure and further improvements resulted in the use of rotating bipole sources at multiple locations in the survey area (Furgerson and Keller, 1974). With these additions, the logistic complexity and the time required to obtain a full set of data in an area are considerably increased.

To facilitate interpretation of the data obtained with either configuration, it is necessary to understand the response patterns obtained in the presence of two-and three-dimensional inhomogeneous geologic models. If the section of interest is homogeneous or uniformly layered, any of the resistivity techniques yield simple responses that are easily understood and interpreted. In most geothermally promising environments, the assumption of a simple layered subsurface is often untenable. The response patterns for the collinear dipole-dipole method to a wide variety of two-and three-dimensional structural models are fairly well understood from various published work based on analog model studies (McPhar Geophysics, 1966, Dey, 1967, Apparao et al, 1969) as well as numerical simulations (e.g. Coggon, 1971, Van Nostrand and Cook, 1966, Dey et al, 1975, Bakbak, 1977, Dieter et al., 1969, Beyer, 1977). The response for the bipole-dipole mapping method, however, is presently understood only for layered earth, single outcropping contact, outcropping dyke with infinite depth-extent with or without an insulating basement (Van Nostrand and Cook, 1966, Vedrintsev, 1966), and for a buried conducting sphere (Singh and Espindola, 1976). Some of these response patterns have been illustrated by Keller et al. (1975) and Doicin (1976). The response of an outcropping hemispherical inhomogeneity was studied by Bibby and Risk (1973). Little information is available (Mazzella and Dey, 1973) to study the response patterns for the bipole-dipole mapping method over buried resistivity inhomogeneities

of simple or complex shapes. Consequently, most of the bipole-dipole mapping data, to date, is interpreted using the tenuous assumption that the section under consideration is uniformly layered and by transforming the mapped data to equivalent Schlumberger expansion sounding curves (Zohdy, 1973).

The purpose of this report is to show the response patterns for the bipole-dipole mapping method for buried two-dimensional inhomogeneities. The effects of depth of burial, source bipole orientation with respect to the strike, overburden layer thickness and conductivity and distance from the transmitting bipole for a single block-shaped conductive target are illustrated. Certain characteristic diagrams are derived for the response of the single inhomogeneity and the responses are compared to those obtained from a collinear dipole-dipole array over identical models. In a following section, a typical North-Central Nevada valley section is simulated with and without the presence of a postulated conductive reservoir. For this structural model, the source bipole is rotated with respect to the strike direction at two different locations and the response patterns for these various configurations are illustrated. A comparative analysis of the response patterns obtained with the collinear dipole-dipole configuration over the same models, is also made.

Definition of the Observed Parameters

The geometric configurations of the collinear dipole-dipole and the bipole-dipole mapping arrays are shown in Figures 1a and 1b, respectively. For a specified geometry of the array the potential difference observed at the receiver dipole is converted to an "apparent resistivity" of the earth. "Apparent resistivity" is a traditional interpretive parameter used in resistivity surveys,

and it indicates the resistivity of an isotropic, homogeneous half-space that would give rise to an identical potential difference for the specific geometry of the array under consideration.

For the collinear dipole-dipole array with a dipole length of a and a dipole-separation of Na, as illustrated in Figure 1a, the apparent resistivity, ρ_a, is defined as

$$\rho_a = \pi N (N+1)(N+2) a \cdot \frac{\Delta V}{I} \qquad (1)$$

For the bipole-dipole mapping configuration, an orthogonal set of roving receiver dipoles, usually oriented parallel and perpendicular to the current bipole, is used to measure the potential differences for a fixed location of the transmitter bipole. A commonly used parameter is an apparent resistivity defined in terms of the magnitude of the total E-field or the total potential difference at a receiver station irrespective of its direction (Risk et al, 1970, Furgerson and Keller, 1974). If the distance to the receiver is large compared to the receiver dipole length and large compared to the transmitting dipole dimension, the potential difference observed at any receiver dipole normalized by its length, is a close approximation to the component of the electric field at the receiver point. The apparent resistivity could be obtained using the magnitude of the resultant electric field, with the formulation given by Keller et al (1975). However, close to the transmitting dipole (within a radius of 3 bipole lengths) such approximations for the point electric field could lead to gross errors. The changes in the curvature of the current lines and the spatial rate of change of the electric field, in this zone, from an equivalent half-space are rather severe, if the receiver dipole length is greater than 1/50th the transmitting bipole length. An equivalent formulation for the apparent resistivity is, however, easily done for small receiver dipoles, using the potential differences, rather than the electric field, in the direction of

each of the orthogonal dipoles. The use of potential differences eliminate the fictitious distortions in calculated apparent resistivity caused by the point electric field approximation made for non-infinitesimal receiver-dipole lengths.

The geometric configuration with the relevant distances for the dipole-dipole mapping array is illustrated in Figure 1b. If ΔV_1 and ΔV_2 are the potential differences measured between the receiver dipoles PP_1 and PP_2, respectively, the apparent resistivity, ρ_a, based on the magnitude of the resultant potential, is given as

$$\rho_a = 2\pi \frac{\sqrt{\Delta V_1^2 + \Delta V_2^2}}{I} \cdot \frac{1}{\sqrt{G_1^2 + G_2^2}} , \qquad (2)$$

where $G_1 = 1/R1 - 1/R3 - 1/R2 + 1/R4,$

and $G_2 = 1/R1 - 1/R3 - 1/R5 + 1/R6.$

In bipole-dipole mapping surveys, when the section under consideration is underlain by a resistive electrical basement, the computation of resistivity based on a cylindrical spreading of current through a thin plate is deemed more appropriate (Keller et al, 1975). With these assumptions, the ratio of plate thickness to resistivity (h/ρ), known as conductance, may be calculated. Using the observed potential differences between the orthogonal pair of dipoles, illustrated in Figure 1b, an "apparent conductance" may be defined as

$$S_a = \frac{I}{2\pi} \cdot \frac{\sqrt{G_3^2 + G_4^2}}{\sqrt{\Delta V_1^2 + \Delta V_2^2}} , \qquad (3)$$

where $G_3 = \log_e (1/R1) - \log_e (1/R3) - \log_e (1/R2) + \log_e(1/R4)$

and $G_4 = \log_e (1/R1) - \log_e (1/R3) - \log_e (1/R5) + \log_e(1/R6)$

It is to be noted that for the bipole-dipole mapping configuration, a measurement parameter similar to apparent resistivity, in concept, could be developed in several other ways. For example, each of the orthogonal receiver dipoles could be individually used to produce two 4-electrode configurations and consequently apparent resistivity maps in two fixed directions (e.g., perpendicular and parallel to the transmitting dipole or to the strike of the geologic section) could be obtained. In addition, since the direction and magnitude of the individual E-fields in two orthogonal directions are known, it is possible to calculate apparent resistivity in the vector E-field direction and at each observation point on the surface the deviation of the current lines from an isotropic homogeneous or a hypothesized layered subsection could be mapped as an additional diagnostic parameter.

In its present day use, the dipole mapping data is routinely reduced as an apparent resistivity and an apparent conductance map using the equations (2) and (3). In routine analysis in this laboratory, the additional parameters indicated above are also evaluated. In this paper, however, the comparative analysis will be made based on the apparent resistivity and apparent conductance obtained from the magnitude of the resultant E-field described above.

Model Computations:

The resistivity response of any arbitrarily shaped two-dimensional geologic section to the collinear dipole-dipole and the dipole-dipole mapping configurations are obtained using a numerical technique (Dey and Morrison, 1976). Finite difference approximations are obtained for the Poissons equation by making a volume discretization of the subsurface. Potential distributions at all points

in the set defining the inhomogeneous half-space are simultaneously obtained for multiple point sources of current injection to an absolute accuracy of better than 5 percent.

In the pseudo-sections and maps described in the following sections, the model dimensions, transmitting and receiving dipole lengths, and the distances in the horizontal and vertical planes are expressed in terms of an arbitrarily scaled unit distance. For routine geothermal exploration, this unit distance could be assumed to be equal to 1 km. Thus for comparison purposes, the dipole lengths in the collinear dipole-dipole configurations are each 1 km in length and dipole separations of up to 10 km are used. For the bipole-dipole mapping method, a transmitting bipole of length 2 km and surrounding areal extent of 20 km x 14 km is used for mapping purposes. In the bipole mapping method, the set of orthogonal receiver dipole pairs is assumed to be oriented parallel and perpendicular to the strike of the geologic section. At each observation point the dipoles are extended in the +y (i.e. strike) and +x (i.e. perpendicular to strike) direction from a common electrode and their lengths are 0.125 times the bipole length. Such a configuration results in a slight assymetry in the maps in regions of positive and negative y-axis values. The apparent conductance values for the bipole-dipole mapping method are normalized by the length of the transmitter (in meters).

Single Conductive Inhomogeneity

A comparison of the response patterns of the two configurations can first be made with a simple model of a buried, single conductive block-shaped inhomogeneity in a half-space. For this purpose, a rectangular conductive block of cross-sectional area 2 km x 2 km is used. The responses of the block inhomogeneity to

the two configurations for various depths of burial, conductivity contrasts and overburden layer conductivities provide significant insight to the anomaly patterns to be expected from simple lateral inhomogeneities. For the bipole-dipole mapping method, the effects of transmitting bipole orientation and distance of the inhomogeneity from the transmitter are also illustrated.

Responses for the bipole-dipole mapping method

Figures 2a and 2b illustrate the apparent resistivity maps obtained with the bipole mapping method over the single rectangular conductor for transmitter orientations perpendicular and parallel to the strike direction, respectively. The resistivity of the surrounding half-space is 100 ohm m and that of the inhomogeneity is 1 ohm m. The depth of burial to the top of the inhomogeneity is 1.0 unit. The transmitting current electrodes are located at (7.0, 0.0) and (5.0, 0.0) for the perpendicular (to strike) orientation and at (-6.0, 0.0) and (-6.0, 2.0), for the parallel orientation, respectively. In the maps illustrated in Figures 2a and 2b, the shallow conductive target is located close to the bipole, the horizontal distance to the center of its projection being 4 units from the center of the transmitter. The apparent resistivity contours show a closed low contour of 30 ohm m for the perpendicular transmitter, and a closed low contour of 20 ohm m for the parallel orientation of the transmitter, that almost directly overlies the projection of the block. The contours indicate a steep decreasing gradient as the near boundary of the target is approached and a rather slow rise past the farther boundary. The resistivity in the region past the body remains at a low value of 55 ohm m for the perpendicular bipole, and 35 ohm m for the parallel bipole, at distances of 11 units past the projection of the conductive inhomogeneity. In the perpendicular orientation of the transmitter, two spurious regions of closed apparent resistivity highs (125 ohm m) are observed to the left of the transmitter

where no resistivity inhomogeneities exist. For the position of the inhomogeneity considered in this example an overlap of the two maps indicate a zone of low resistivity coincident with the location of the target with good resolution.

The apparent conductance maps for this location of the conductive target are presented in Figures 3a and 3b, for the transmitter orientations perpendicular and parallel to the strike, respectively. In the absence of an insulating basement, the apparent conductance parameter does not have any physical significance. However, the computed parameter shows generally high apparent conductance values over the projection of the target. In the parallel bipole orientation, the highest value is reached in regions shifted considerably farther from the projection of the target.

In order to illustrate the effect of increasing distance of the bipole from the projection of the conductive target, the block-shaped inhomogeneity was shifted to the right to a position between +1 and +3 units in the x-direction and at an identical depth of burial of 1 unit. The transmitting bipoles were located at the same positions as in the previous example. The apparent resistivity maps for the bipoles oriented perpendicular and parallel to the strike direction are shown in Figures 4a and 4b, respectively. A comparison with Figures 2a and 2b indicates the appearance of further spurious closed high and low resistivity contours for the perpendicular bipole to the left of the transmitter. The target location is indicated with good lateral resolution, for the perpendicular bipole, with a closed low resistivity contour of 30 ohm m. The lowest closed contour of 30 ohm m, obtained for the parallel bipole, however, shows a shift farther away from the projection of the far boundary of the target. The apparent conductance maps for this model, shown in Figures 5a and 5b for the perpendicular and parallel bipole orientations, indicate steep gradients with increasing conductance values towards the near edge of the conductor. The resolution in defining the width of the target in this location seems to be worse for the parallel orientation of the transmitting

bipole than for the perpendicular.

Figures 6a and 6b illustrate the apparent resistivity response patterns for the perpendicular and parallel configurations of the transmitter with the conductive block located in close proximity to the bipole but at a greater depth of burial, as shown in the accompanying section. The apparent resistivity anomalies are considerably broadened and are bounded by much shallower gradients in the contour levels (compared to Figures 2a and 2b). The lateral resolution in the location of the target is very poor, in that the shallow low resistivity trough is approximately 7-8 units in width and is considerably displaced away from the projection of the conductive block. The apparent conductance maps obtained for the model with perpendicular and parallel orientations of the bipole are illustrated in Figures 7a and 7b, respectively. No diagnostic pattern emerges for either map, with the conductance values monotonically increasing away from the transmitter towards the right edge of the map.

Response for the collinear dipole-dipole profiling method

The standard pseudo-section plots of the apparent resistivity response for the collinear dipole-dipole array are illustrated in Figures 8a and 8b, for the 2 unit x 2 unit conductive block located at depths of burial of 1 and 2 units, respectively. The length of each of the transmitting and receiving dipoles is 1 unit and the pseudo-section is plotted with dipole-separations N = 1, 2, 3.....10. The conductive inhomogeneity is of intrinsic resistivity 1 ohm m and the surrounding half-space has a resistivity of 100 ohm m. A higher degree of spatial resolution in terms of the horizontal location of the conductive target at both depths is evident from the simple patterns in the pseudo-section. For the shallow location of the block, the effect of its finite depth-extent is clearly indicated by the closed

low resistivity contour underlain by increasing resistivity. For the deeper target, the depth to top is easily estimated, however, with dipole-separations up to N = 10, the depth extent of the target cannot be estimated. The considerably improved spatial resolution and well-defined anomaly pattern indicate the enhanced diagnosticity achievable with multiple transmitter locations in a profile mode. Their pseudo-section contour patterns are well-defined for simple structures and indicate predictable variations with changing conductivity contrasts, depths of burial, etc. Hence, for such simple shapes, unlike bipole-dipole mapping results, only a few model iterations produce the desired interpretation.

Characteristic curves for the single, rectangular conductive Block Inhomogeneity

The apparent resistivity responses obtained by emplacing the 2 unit x 2 unit conductive block at various depths of burial and by changing its conductivity contrast with respect to the surrounding half-space, for bipole-dipole and dipole-dipole configurations, are summarized in the characteristic diagram shown in Figure 9. A normalized anomaly index is defined as

$$A.I. = \frac{\rho_{a^{max}} - \rho_{a^{min}}}{\rho_{background}} \times 100\%$$

In the pseudo sections and in the background apparent resistivity surface maps there appear zones of apparent resistivity high as well as low, due to the presence of a conductive target. If the subsurface were to be isotropic and homogeneous, the apparent resistivity parameter observed with either configuration would have been the intrinsic resistivity of the half-space. In this characteristic diagram, A. I., the anomaly index, is a measure of the distortions produced in a half-space response due to the presence of the lateral inhomogeneity. For this diagram, the conductivity contrasts $\sigma_{body}/\sigma_{half\ space}$ of 10 and 100 and depth

of burial varying for 0.5 units to 3 units are considered. The transmitter orientations and the horizontal projection of the target with respect to the bipoles are identical to those shown in Figures 2a and 2b. It is evident from Figures 4a, 4b and 6a, 6b that, depending on the distance and orientation of the bipoles, the amplitude and location of the spurious closed highs vary, thus resulting in considerable variation in their corresponding A.I measure.

The curves shown in Figure 9 indicate that the peak to peak anomaly observed with a bipole-dipole map (for the perpendicular orientatation of the transmitter) in generally higher than that obtained for the collinear dipole-dipole, for the same model. In practical implementation, however, a technique would be best suited if a higher A.I. in the overall map is combined with a high degree of lateral resolution, so that the target location and dimensions could be easily interpreted. From the anomaly patterns illustrated thus far, it is apparent that the collinear dipole-dipole array is superior in this regard.

Effect of Conductive Overburden Layers

Bipole-Dipole Mapping Response:

The effect of relatively thin conducting overburden layers over the standard conductive shallow inhomogeneity located close to the bipoles is illustrated in Figures 10a and 10b, for the perpendicular and parallel orientations of the bipole, respectively. The overburden layer resistivity is 10 ohm m and the layer thickness is 0.125 of the bipole length used. In the vicinity of the bipoles, the typical response from two-layered earth models is seen for both orientations. A comparison with Figures 2a and 2b, however, indicates that even for the shallow depth of burial and close proximity of the target to the bipoles, the associated low resistivity contours are reduced in amplitude and broadened. With the presence

of the overburden layer, the parallel orientation of the bipole seems to yield a better definition of the target location. The lateral location of the target as indicated by the 40 ohm m closed contour in both maps is poorly defined.

The apparent conductance maps for this model are shown in Figures 11a and 11b, for the two bipole orientations. While the conductance concept is more realistic for these layered models, no diagnostic pattern emerges. For the parallel bipole configuration there is an associated conductance high close to the surface projection of the conductive target.

Collinear dipole-dipole response:

The response of the 2 unit x 2 unit conductor located at a depth of 1 unit below the surface and overlain by a conductive overburden layer of thickness 0.25 km and intrinsic resistivity of 10 ohm m, is illustrated in the pseudo-section shown in Figure 12. The patterns in the pseudo-section away from the lateral inhomogeneity indicate the typical two-layered responses. Over the region of the target, its location and lateral bounds are well defined. The relative resistivity high occurring at large dipole-separation in the center of the section indicates the finite depth extent of the conductive target. The typical pseudo-section pattern, thus enables easy interpretation for both the location of the target and the resolution of the overburden layer conductivity and thickness.

In the course of this study many other simple block models were simulated. Using a 2 unit x 2 unit conductive block at a depth of one unit, the bipole-dipole mapping method showed poor detection capability (i.e., A.I. measures of less than 5%) in the following cases:

1) for horizontal distances between the block and the transmitter in excess of 6 units.
2) for overburden layer thicknesses in excess of 0.5 units, with overburden layer conductivity 10 times that of the lower half space.

Another example of the inherent ambiguity of the bipole-dipole maps is the comparison of the buried conductive block of Figure 6a with a buried conductive quarter space, (Figure 13). Not only are the patterns for these two radically different models quite similar, but the range of the apparent resistivities is very nearly the same. The apparent resistivity gradients for both models in the right half of the section are also similar.

All of these ambiguities are simply explained by considering the variation that exists along single diagonals in the dipole-dipole pseudo-sections. Each of these represents the apparent resistivity observed in sections collinear with a single bipole location. To illustrate this effect we can consider the diagonals from two specific transmitter locations, T_1 and T_2, shown in Figure 8 (buried block pseudo-section) and Figure 14 (buried quarter space pseudo-section), respectively. The apparent resistivities along the diagonals to the right of each transmitter are similar and give no clue as to the true conductivity structure. Of course, the fortuitous addition of a second bipole transmitter could reduce this ambiguity, but a priori information would be required for optimum field location of this transmitter. The dipole-dipole pseudo-sections resolve these models very well.

In an attempt to reduce the bipole-dipole data to a more interpretable form, we investigated the effects of subtracting assumed half-space or layered half-space models from models containing inhomogeneities. Initially, it seemed reasonable that anomalies from buried electrical inhomogeneities could be enhanced if we were to first calculate the anomaly for the estimated layered structure and subtract this from the observed data. An example of efforts to test this concept is shown in Figure 15. The upper map (Figure 15a) shows the effect of a rectangular inhomogeneity buried beneath an overburden layer when energized by the perpendicular bipole. After subtracting the calculated effect

of the layering only (Figure 15b) we obtained the so-called residual anomaly shown in Figure 15c. Figure 15c is not indicative of a bounded inhomogeneity and in fact has the pattern of a buried conductive quarter-space (see Figure 13). Attempts to interpret residual maps for more complicated geology met with even less success.

Comparative Response patterns over more Complex Geologic Sections

The response patterns have been presented for a single conductive inhomogeneity with and without the presence of a conductive overburden. It is generally observed that even for the simplest geometries, the bipole-dipole map has highly complex, non-definitive, patterns of apparent resistivity and conductance. For the identical sub-surface inhomogeneity, conflicting overlays of apparent resistivity patterns are obtained depending on the location and orientation of the transmitting bipoles.

In order to evaluate the practical effectiveness of the bipole-dipole and dipole-dipole techniques in an area of geothermal potential, where the geologic section is often considerably more complex, the methods were applied to two hypothetical Central Nevada Basin-and-Range type electrical cross-sections. Structure A (Figure 16) shows the electrical section of a typical valley and Structure B (Figure 17) is the same section with a postulated geothermal reservoir of dimension 1.5 km x 3.0 km and resistivity 1 ohm m.

The pseudo-section plots of the apparent resistivity responses obtained from the models structure A and structure B are shown in Figures 18 and 19, respectively. In Figure 18, the location of the bounding range faults (shown in Figure 16) are clearly seen. In the central part of the pseudo-section, the relatively flat and uniform pattern at dipole-separations up to N = 5, indicates a

layered valley structure. The pseudo-section in Figure 19 also indicates the bounding faults with good resolution, but the pattern in the central part, at dipole separations 2 to 10, shows a zone of relatively low apparent resistivity indicating the presence of a large, bounded conductive zone at depth. A comparison of the 8 ohm m contour of Figure 19 and the 13 ohm m. contour of Figure 18 shows that one could infer the location of the low-resistivity reservoir zone in Figure 19 without prior knowledge of the valley structure.

Bipole-dipole mapping responses, calculated in terms of apparent resistivity and conductance, are given for both structures A and B. Current bipoles at two locations, centered at x = -3.5 and x = +3.5 (Figures 16, 17), were chosen. At each location, transmitting bipoles approximately 2 km in length were oriented at angles 0°, 45°, 90° and 135° to the strike of the section. The apparent resistivity and conductance maps with the exact location and orientations of the bipole sources are illustrated in Figures 20 to 27 for structure A and in Figures 28 to 35 for structure B (with the postulated reservoir zone).

A comparative study of these maps indicates a layered sub-section very close to the current electrodes, for the parallel and perpendicular orientation of the bipoles. The range front contacts with large resistivity contrasts are outlined rather well by the bipole oriented parallel to the strike. For any other azimuthal orientation of the bipole, either east or west of the center of the section, the fault contact located farther away is more clearly seen. The effect of the nearer (to the transmitter) contact is subtle for the perpendicular orientation and often obscured for azimuthal angles of 45° or 135°. Although the basement in the central part of the valley is electrically resistive, no definitive pattern emerges in the conductance maps to estimate basement depth with good resolution.

A comparison of the responses in the sets of Figures 20-27 with those in Figure 28-35 does not indicate a sharp change in the resistivity, or reveal diagnostic resistivity or conductance pattern changes that can be used to determine the location of the large low resistivity reservoir zone. The two sets of patterns are virtually the same and only with an a priori knowledge of structure A, could the subtle changes in the low values of resistivity maps in the central part be correlated with the presence of the conductive reservoir zone.

Conclusions

Based on analyses of the models included in this report and on a wide variety of models which we have used in attempts to model field data, the following conclusions may be drawn:

1) Multiple sources are required to determine the subsurface resistivity distribution with the bipole-dipole configuration. There is a constant gain in information as the number of sources approaches that of a complete dipole-dipole pseudo-section. Definitive patterns required to differentiate radically different models do not, in general, appear from only two transmitter position.
2) The bipole-dipole method appears to be effective for locating shallow bounded conductive targets, especially if these targets are within two or three bipole lengths from the transmitter.
3) The bipole-dipole method is good for locating outcropping dikes or contacts, for any orientation of the bipole, and especially at large distances from the transmitter.
4) Conductive overburden severely supresses the anomalies from conductive inhomogeneities. Patterns for anomaly recognition of lateral inhomogeneities

are not definitive even for multiple sources.

5) Except when located in very close proximity of the bipole, the bipole-dipole maps show extremely poor resolution in defining the width and the depth extents of bounded inhomogeneities.

6) Surface inhomogeneities contribute large distortions with bipole-dipole maps. The dipole-dipole pseudo-sections allow recognition and some differentiation of these features.

7) Except for some very simple geometries, bipole-dipole maps for varying bipole orientations (rotations) present little additional information.

8) The subtle difference in apparent resistivity maps that characterize different conductivity structures would require a very high density of receiving dipoles.

9) In view of the requirements of multiple transmitters and a high density of receiver dipoles it is not clear that the bipole-dipole technique can offer any cost advantages over spot Schlumberger soundings or select dipole-dipole profiles.

10) For the models studied, high conductances corresponded generally with low apparent resistivities. The patterns of the conductance maps did not add any diagnostic information.

11) Except in very special geologic settings, e.g., outcropping faults and dykes, the effectiveness of the bipole-dipole technique as a reconnaissance mapping tool for the location of conductive zones is very poor.

Acknowledgement

The authors are indebted to Juan Parra for computational assistance. Support for this work has been provided by the United States Energy Research and Development Administration through Lawrence Berkeley Laboratory.

List of Figures

Figure 10 - Bipole-dipole apparent resistivity maps over a single, shallow inhomogeneity with a conductive overburden with the current bipole oriented a) perpendicular and b) parallel to the strike.

Figure 11 - Bipole-dipole apparent conductance maps over a single, shallow inhomogeneity with a conductive overburden with a current bipole oriented a) perpendicular and b) parallel to the strike.

Figure 12 - Dipole-dipole apparent resistivity pseudo-section over a single, shallow inhomogeneity with a conductive overburden.

Figure 13 - Bipole-dipole apparent resistivity map over a buried conductive quarter-space with the current bipole perpendicular to the strike.

Figure 14 - Dipole-dipole apparent resistivity pseudo-section over a buried conductive quarter-space.

Figure 15 - Bipole-dipole apparent resistivity maps a) over a conductive inhomogeneity with a conductive overburden layer, b) over the two-layered earth, and c) the residual with the current bipole oriented parallel to the strike.

Figure 16 - A resistivity cross-section of a typical North Central Nevada Valley section (Structure A).

Figure 17 - A resistivity cross-section of a typical North Central Nevada Valley section with a hypothesized conductive zone (Structure B).

Figure 18 - Dipole-dipole apparent resistivity pseudo-section over the valley structure A.

Figure 19 - Dipole-dipole apparent resistivity pseudo-section over the valley structure B.

Figure 20 - Bipole-dipole apparent resistivity maps over the valley structure A with the current bipole at (-3.5,0) and oriented a) perpendicular, and b) parallel to the strike direction.

Figure 21 - Bipole-dipole apparent conductance maps over the valley structure A with the current bipole at (-3.5,0) and oriented a) perpendicular and b)

parallel to the strike direction.

Figure 22 - Dipole-dipole apparent resistivity maps over the valley structure A with the current bipole located at (-3.5,0) and oriented at a) 45 degrees, and b) 135 degrees to the strike direction.

Figure 23 - Bipole-dipole apparent conductance maps over the valley structure A with current bipole located at (-3.5,0) and oriented at a) 45 degrees and b) 135 degrees to the strike direction.

Figure 24 - Bipole-dipole apparent resistivity maps over the valley structure A with the current bipole located at (+3.5,0) and oriented a) perpendicular, and b) parallel to the strike direction.

Figure 25 - Bipole-dipole apparent conductance maps over the valley structure A with the current bipole located at (+3.5,0) and oriented a) perpendicular, and b) parallel to the strike direction.

Figure 26 - Bipole-dipole apparent resistivity maps over the valley structure A with the current bipole located at (+3.5,0) and oriented at a) 45 degrees and b) 135 degrees to the strike direction.

Figure 27 - Bipole-dipole apparent conductance maps over the valley structure A with the current bipole located at (+3.5,0) and oriented at a) 45 degrees and b) 135 degrees to the strike direction.

Figure 28 - Bipole-dipole apparent resistivity maps over the valley structure B with the current bipole at (-3.5,0) and oriented a) perpendicular and b) parallel to the strike direction.

Figure 29 - Bipole-dipole apparent conductance maps over the valley structure B with the current bipole at (-3.5,0) and oriented a) perpendicular and b) parallel to the strike direction.

Figure 30 - Bipole-dipole apparent resistivity maps over the valley structure B with the current bipole located at (-3.5,0) and oriented at a) 45 degrees and b) 135 degrees to the strike direction.

Figure 31 - Bipole-dipole apparent conductance maps over the valley structure B with the current bipole located at (-3.5,0) and oriented at a) 45 degrees and b) 135 degrees to the strike direction.

Figure 32 - Bipole-dipole apparent resistivity maps over the valley structure B with the current bipole located at (+3.5,0) and oriented a) perpendicular and b) parallel to the strike direction.

Figure 33 - Bipole-dipole apparent conductance maps over the valley structure B with the current bipole located at (+3.5,0) and oriented a) perpendicular and b) parallel to the strike direction.

Figure 34 - Bipole-dipole apparent resistivity maps over the valley structure B with the current bipole located at (+3.5,0) and oriented at a) 45 degrees and b) 135 degrees to the strike direction.

Figure 35 - Bipole-dipole apparent conductance maps over the valley structure B with the current bipole located at (+3.5,0) and oriented at a) 45 degrees and b) 135 degrees to the strike direction.

References

Apparao, A., Roy, A., and Mallick, K., 1969, Resistivity model experiments: Geoexploration, vol. 7, p. 45.

Bakbak, R., 1977, Three-dimensional numerical modelling in resistivity and IP prospecting: Ph.D. thesis, University of California, Berkeley.

Beyer, H., 1977, Telluric and d.c. resistivity techniques applied to the geophysical investigation of Basin and Range Geothermal Systems, Part II: A numerical model study of the dipole-dipole and Schlumberger resistivity methods, Lawrence Berkeley Laboratory Report no. LBL-6325-2/3.

Bibby, H.M., and Risk, G.F., 1973, Interpretation of dipole-dipole resistivity surveys using a hemispheroidal model: Geophysics, vol. 41, p. 742.

Coggon, J.H., 1971, Electromagnetic and electrical modeling by the finite element method: Geophysics, vol. 36, p. 132.

Dey, A., 1969, Model studies on electrical profiling over thick conducting veins: M.Sc. thesis, Indian Institute of Technology, Kharagpur.

Dey, A., Meyer, W.H., Morrison, H.F., and Dolan, W.M., 1975, Electric field response of two-dimensional inhomogeneities to unipolar and bipolar electrode configurations: Geophysics, vol. 40, p. 630.

Dey, A., and Morrison, H.F., 1976, Resistivity modeling for arbitrarily shaped two-dimensional structures, Part 1: Theoretical Formulation, Lawrence Berkeley Laboratory Report no. LBL-5223.

Dieter, K., Paterson, N.R., and Grant, F.S., 1969, IP and resistivity type curves for three dimensional bodies: Geophysics, vol. 34, p. 615.

Doicin, D., 1976, Quadripole-quadripole arrays for direct current measurements: Geophysics, vol. 41, p. 79.

Furgerson, R., and Keller, G.V., 1974, Computed dipole resistivity effects for an earth model with vertical and lateral contrasts in resistivity: Off. Naval Res. Rep. of Investigations, Colorado School of Mines.

Hallof, P., 1957, On the interpretation of resistivity and induced polarization results: Ph.D. thesis, M.I.T., Department of Geology and Geophysics.

Heiland, C.A., 1940, Geophysical Exploration, New York, Prentice Hall.

Keller, G.V., Furgerson, R., Lee, C.Y., Harthil, N., and Jacobson, J.J., 1975, The dipole mapping method: Geophysics, vol. 40, p. 451.

Mazzella, A., and Dey, A., 1973, A comparative study of two resistivity techniques as applied in the delineation of a geothermal reservoir (abstract): Geophysics, vol. 38, p. 1212.

McPhar Geophysics, 1967, Catalogue of resistivity and IP model data, McPhar Geophysics Ltd., Ontario, Canada.

Risk, G.F., Macdonald, W.J.P., and Dawson, C.B., 1970, D.C. Resistivity surveys of the Broadlands Geothermal Region, New Zealand: Geothermics, Spec. Issue 2, vol. 2, p. 287.

Singh, S.K., and Espindola, J.M., 1976, Apparent resistivity of a perfectly conducting sphere buried in a half-space: Geophysics, vol. 41, p. 742.

Stanley, E.D., Jackson, D.B., and Zohdy, A.A.R., 1976, Deep electrical investigations in the Long Valley geothermal area, California: Journal of Geophysical Research, vol. 81, no. 5, p. 801.

Van Nostrand, R.G., and Cook, R.K., 1966, Interpretation of resistivity data, U.S.G.S., Prof. Paper 499.

Vedrintsev, G.A., 1966, Theory of electric sounding in a medium with lateral discontinuities, in Dipole Method for Measuring Earth Conductivity: Consult Bureau, New York, p. 115.

Zohdy, A.A.R., 1973, Total field resistivity mapping (abstract): Geophysics, vol. 38, p. 1231.

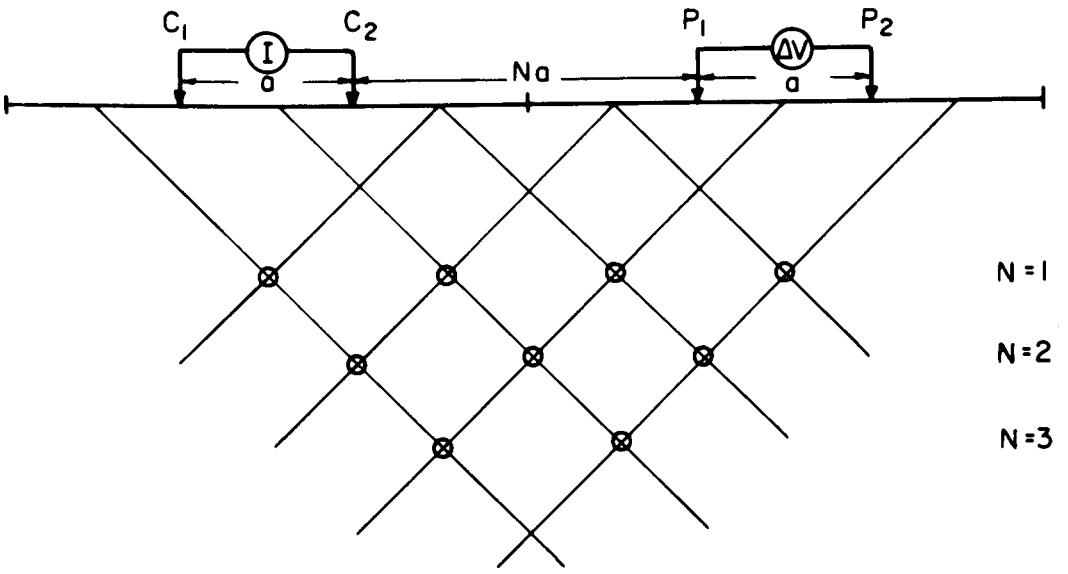

(a) COLLINEAR DIPOLE-DIPOLE CONFIGURATION

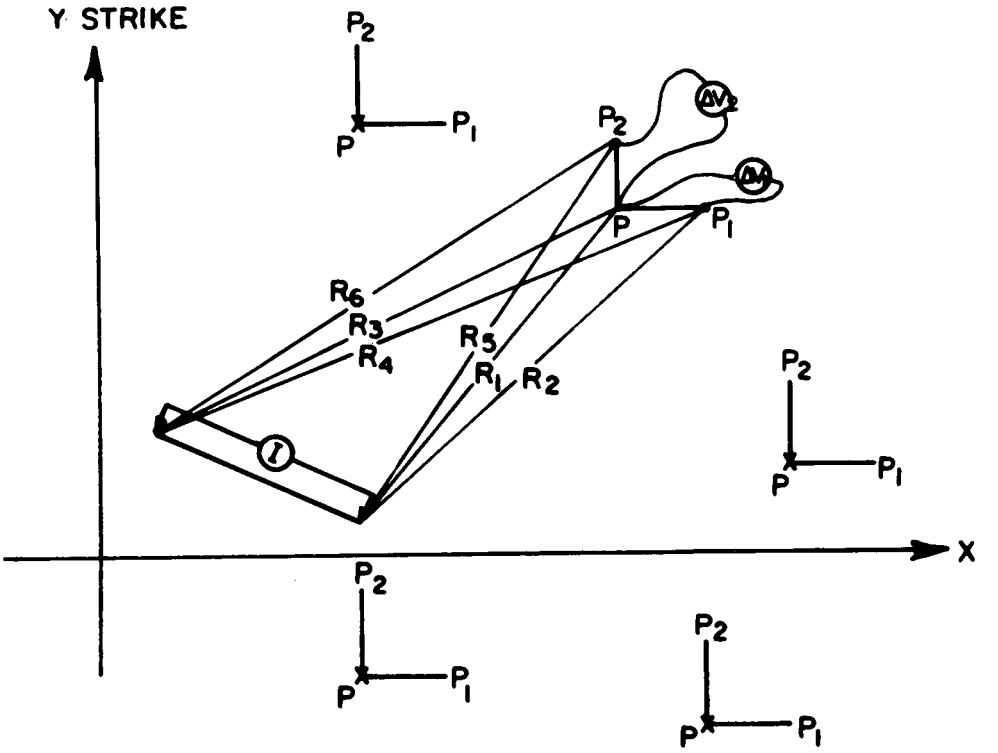

(b) BIPOLE-DIPOLE MAPPING CONFIGURATION

Figure 1

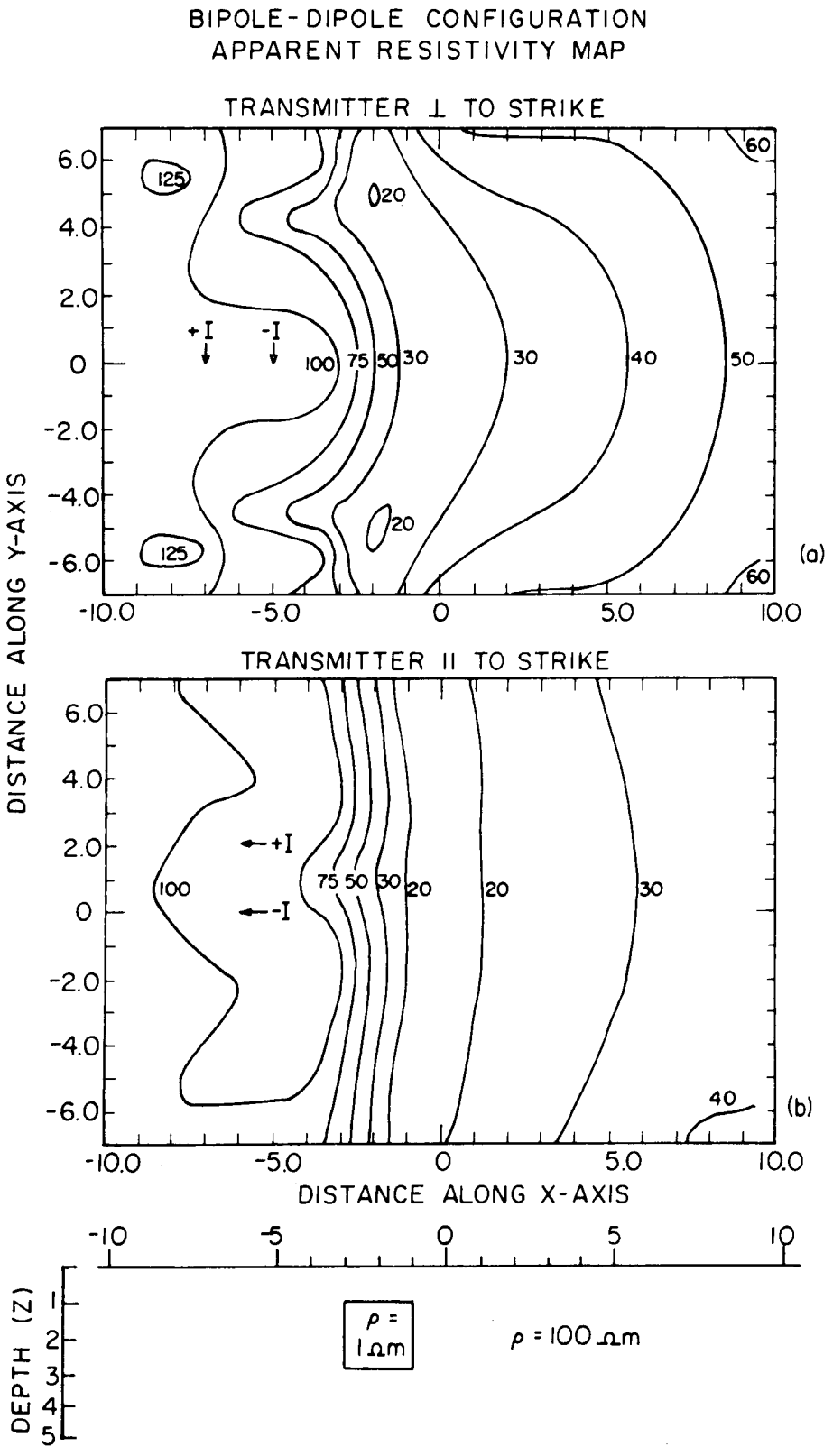
BIPOLE-DIPOLE CONFIGURATION
APPARENT RESISTIVITY MAP
TRANSMITTER ⊥ TO STRIKE
TRANSMITTER ∥ TO STRIKE
DISTANCE ALONG Y-AXIS
DISTANCE ALONG X-AXIS
DEPTH (Z)
+I
-I
125
100
75
50
30
20
60
40
(a)
(b)
ρ = 1 Ωm
ρ = 100 Ωm

Figure 2

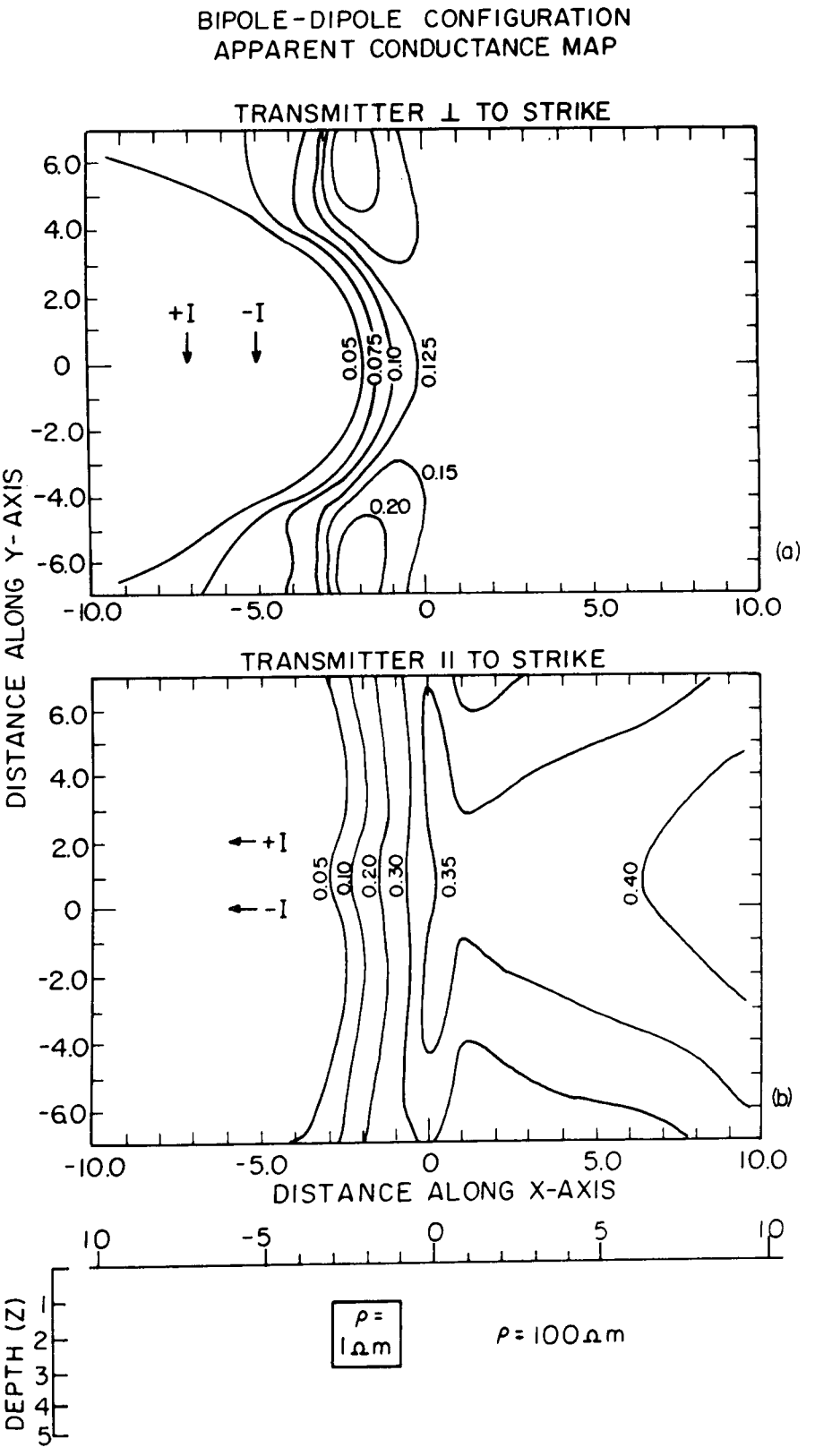
BIPOLE-DIPOLE CONFIGURATION
APPARENT CONDUCTANCE MAP
TRANSMITTER ⊥ TO STRIKE
+I
-I
0.05
0.075
0.10
0.125
0.15
0.20
(a)
TRANSMITTER II TO STRIKE
+I
-I
0.05
0.10
0.20
0.30
0.35
0.40
(b)
DISTANCE ALONG Y-AXIS
6.0
4.0
2.0
0
-2.0
-4.0
-6.0
-10.0
-5.0
0
5.0
10.0
DISTANCE ALONG X-AXIS
10
-5
0
5
10
DEPTH (Z)
1
2
3
4
5
ρ = 1Ωm
ρ = 100Ωm

Figure 3

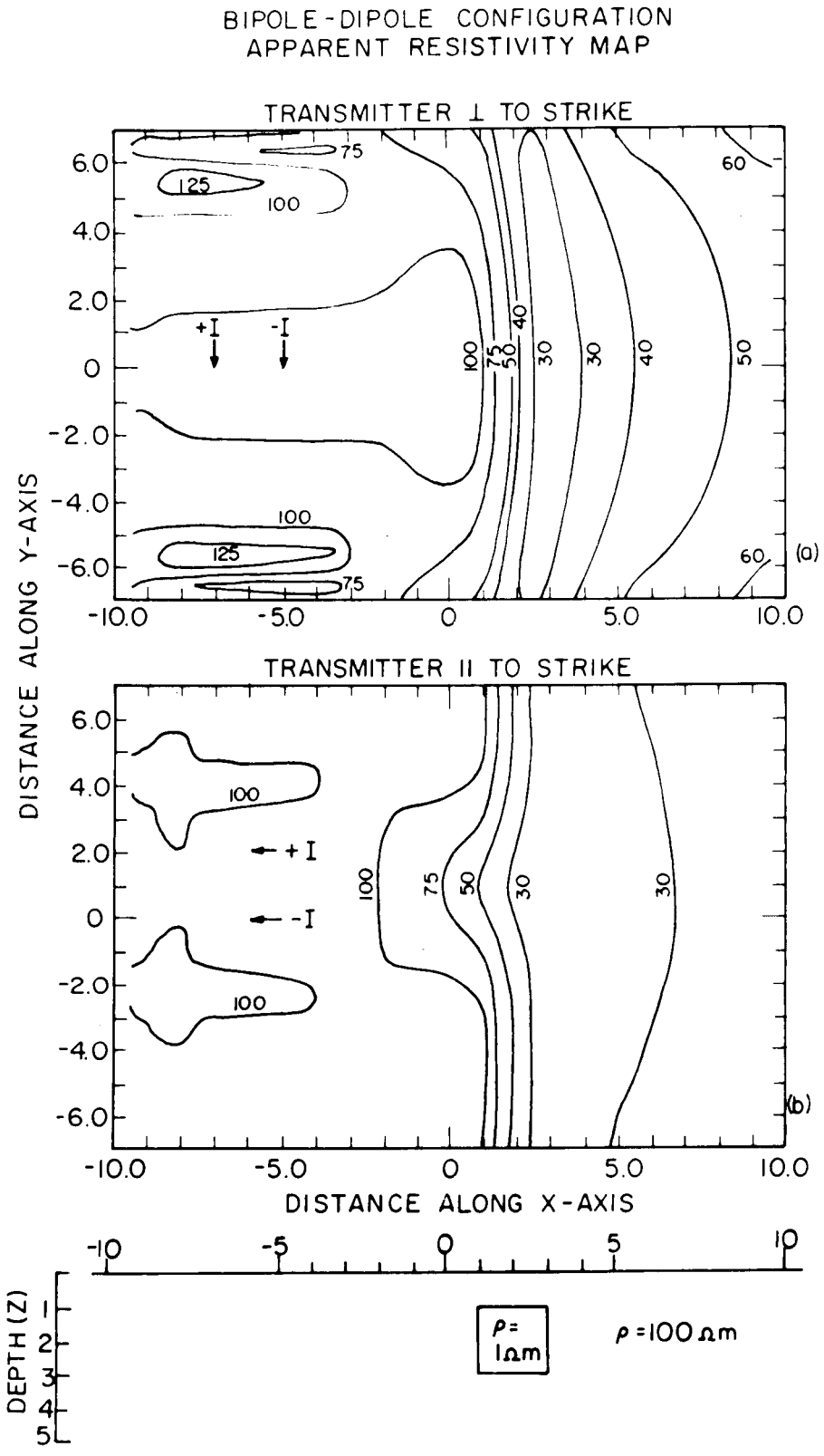
BIPOLE-DIPOLE CONFIGURATION
APPARENT RESISTIVITY MAP
TRANSMITTER ⊥ TO STRIKE
TRANSMITTER ∥ TO STRIKE
DISTANCE ALONG Y-AXIS
DISTANCE ALONG X-AXIS
DEPTH (Z)
+I
-I
(a)
(b)
ρ= 1Ωm
ρ =100 Ωm

Figure 4

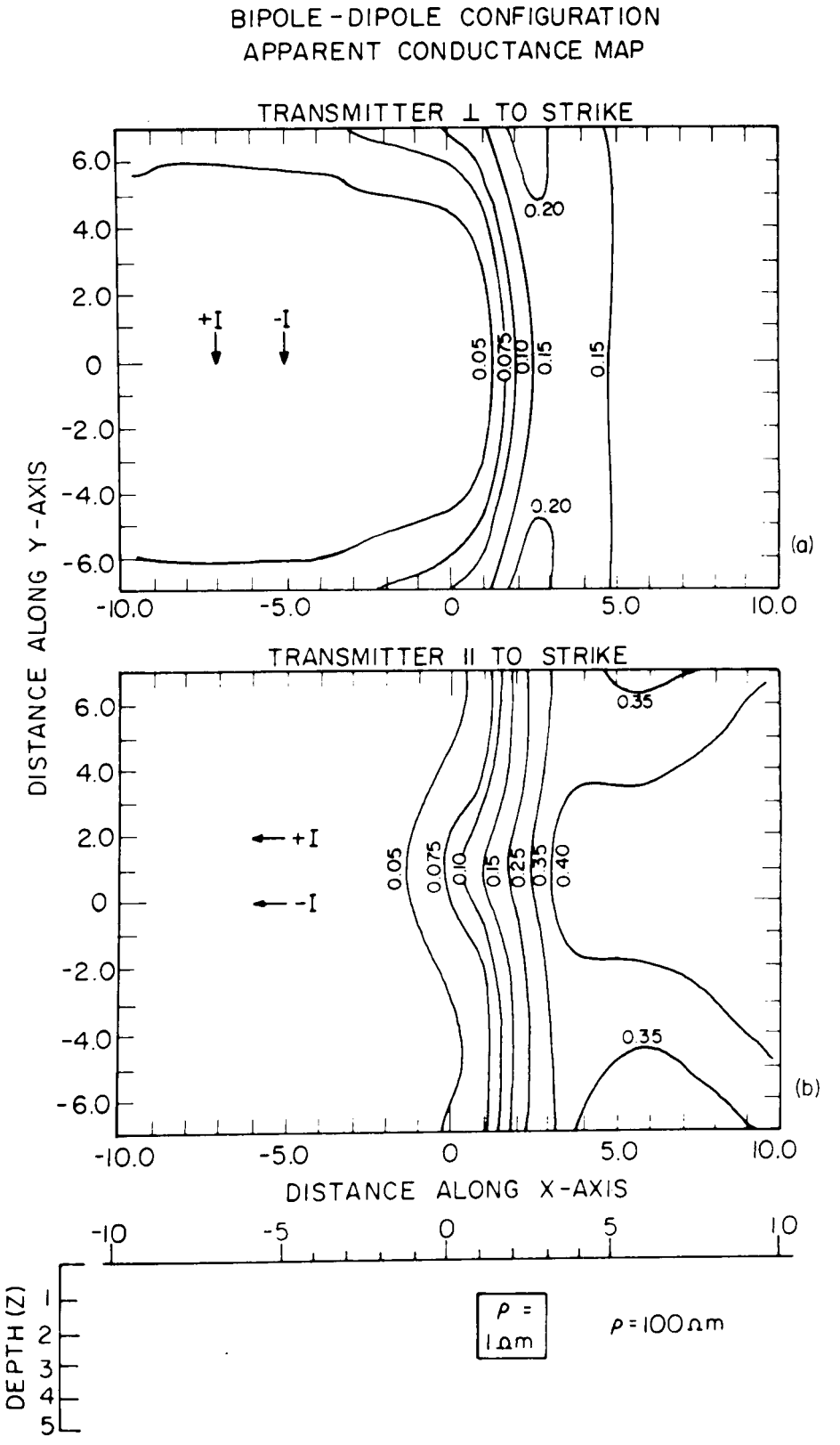
BIPOLE - DIPOLE CONFIGURATION
APPARENT CONDUCTANCE MAP
TRANSMITTER ⊥ TO STRIKE
TRANSMITTER ∥ TO STRIKE
DISTANCE ALONG Y-AXIS
DISTANCE ALONG X-AXIS
DEPTH (Z)
+I
-I
0.05
0.075
0.10
0.15
0.20
0.25
0.35
0.40
(a)
(b)
ρ = 1Ωm
ρ = 100Ωm

Figure 5

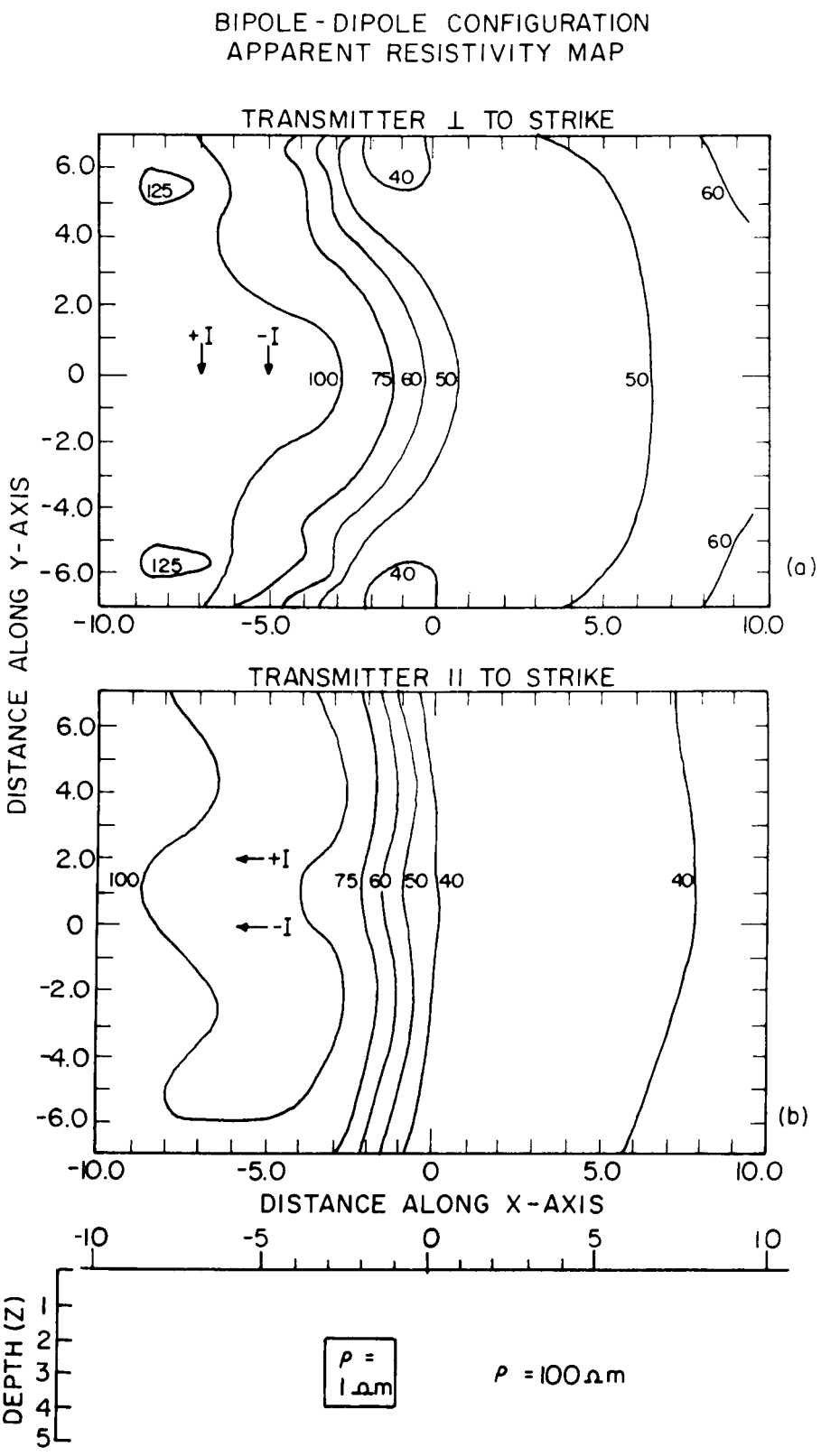
BIPOLE - DIPOLE CONFIGURATION
APPARENT RESISTIVITY MAP
TRANSMITTER ⊥ TO STRIKE
TRANSMITTER ∥ TO STRIKE
DISTANCE ALONG Y-AXIS
DISTANCE ALONG X-AXIS
DEPTH (Z)
+I
-I
125
40
60
100
75
50
(a)
(b)
ρ = 1 Ωm
ρ = 100 Ωm

Figure 6

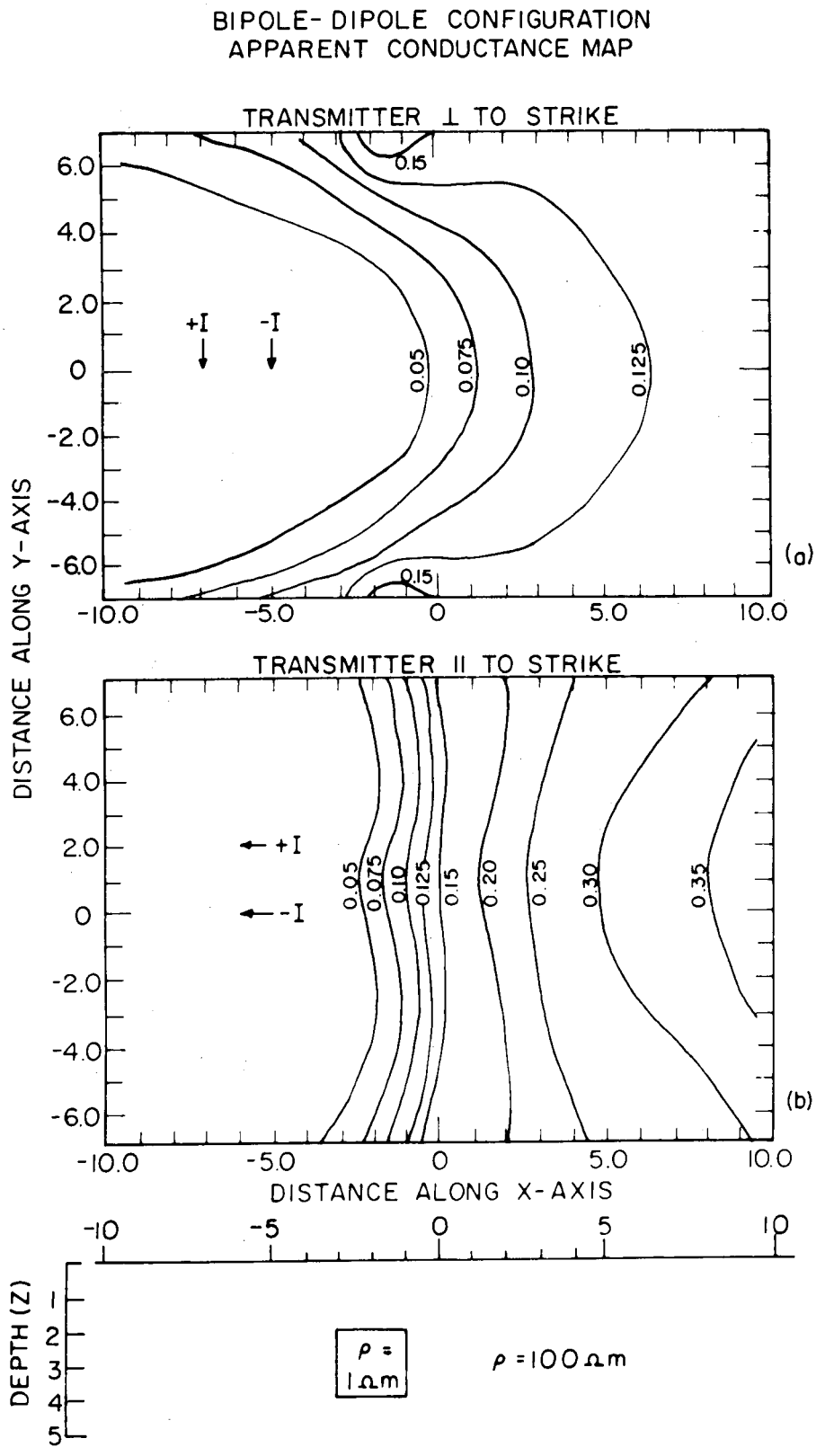
BIPOLE-DIPOLE CONFIGURATION
APPARENT CONDUCTANCE MAP
TRANSMITTER ⊥ TO STRIKE
TRANSMITTER ∥ TO STRIKE
DISTANCE ALONG Y-AXIS
DISTANCE ALONG X-AXIS
DEPTH (Z)
+I
-I
0.05
0.075
0.10
0.125
0.15
0.20
0.25
0.30
0.35
(a)
(b)
ρ = 1 Ωm
ρ = 100 Ωm

Figure 7

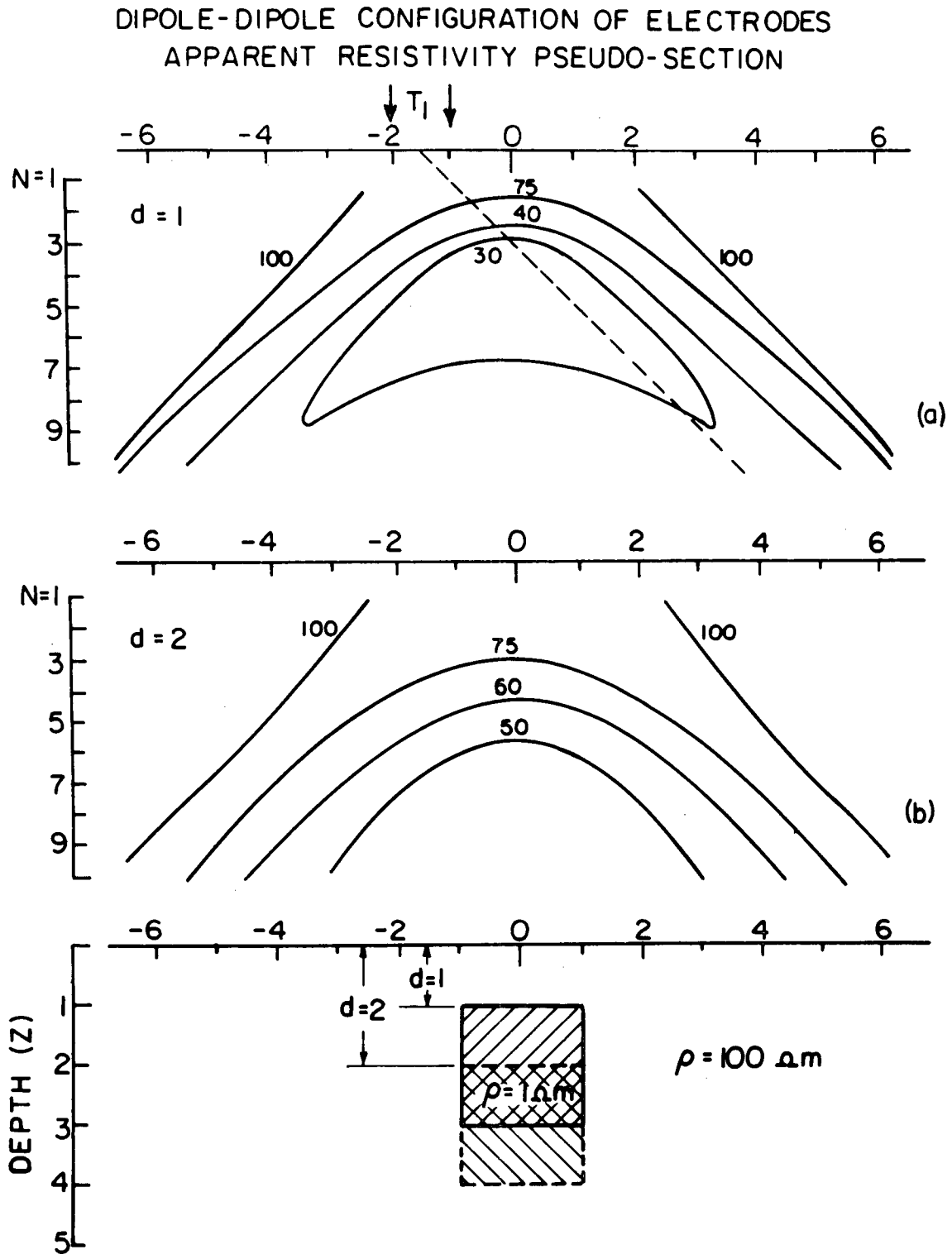
DIPOLE-DIPOLE CONFIGURATION OF ELECTRODES
APPARENT RESISTIVITY PSEUDO-SECTION
T1
-6
-4
-2
0
2
4
6
N=1
3
5
7
9
d = 1
75
40
30
100
100
(a)
d = 2
60
50
(b)
DEPTH (Z)
1
2
3
4
5
d=1
d=2
ρ = 100 Ω m
ρ = 1 Ω m

Figure 3

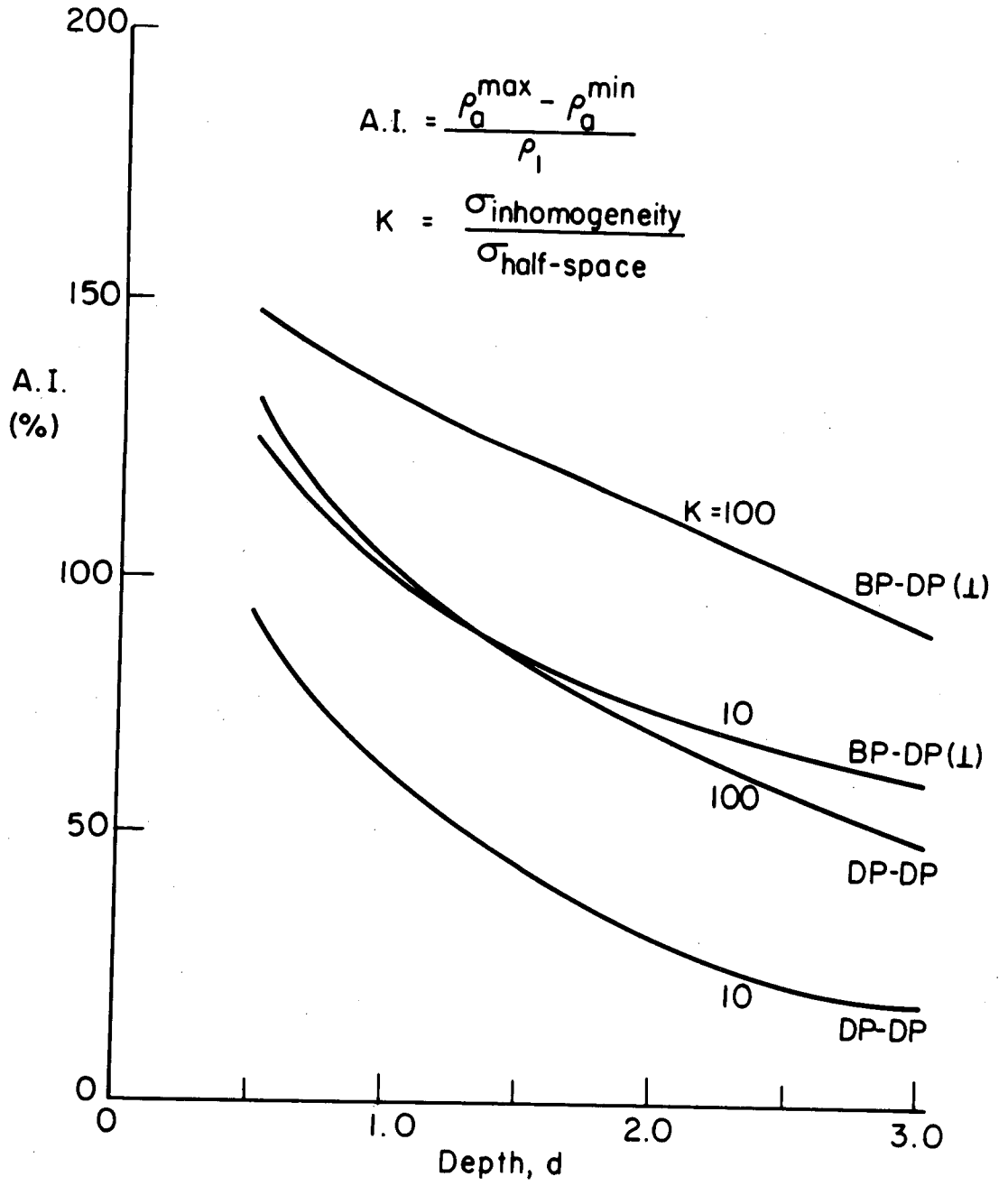
200
150
100
50
0
A.I.
(%)
$A.I. = \frac{\rho_a^{max} - \rho_a^{min}}{\rho_1}$
$K = \frac{\sigma_{inhomogeneity}}{\sigma_{half\text{-}space}}$
K =100
BP-DP (⊥)
10
BP-DP (⊥)
100
DP-DP
10
DP-DP
0
1.0
2.0
3.0
Depth, d

Figure 9

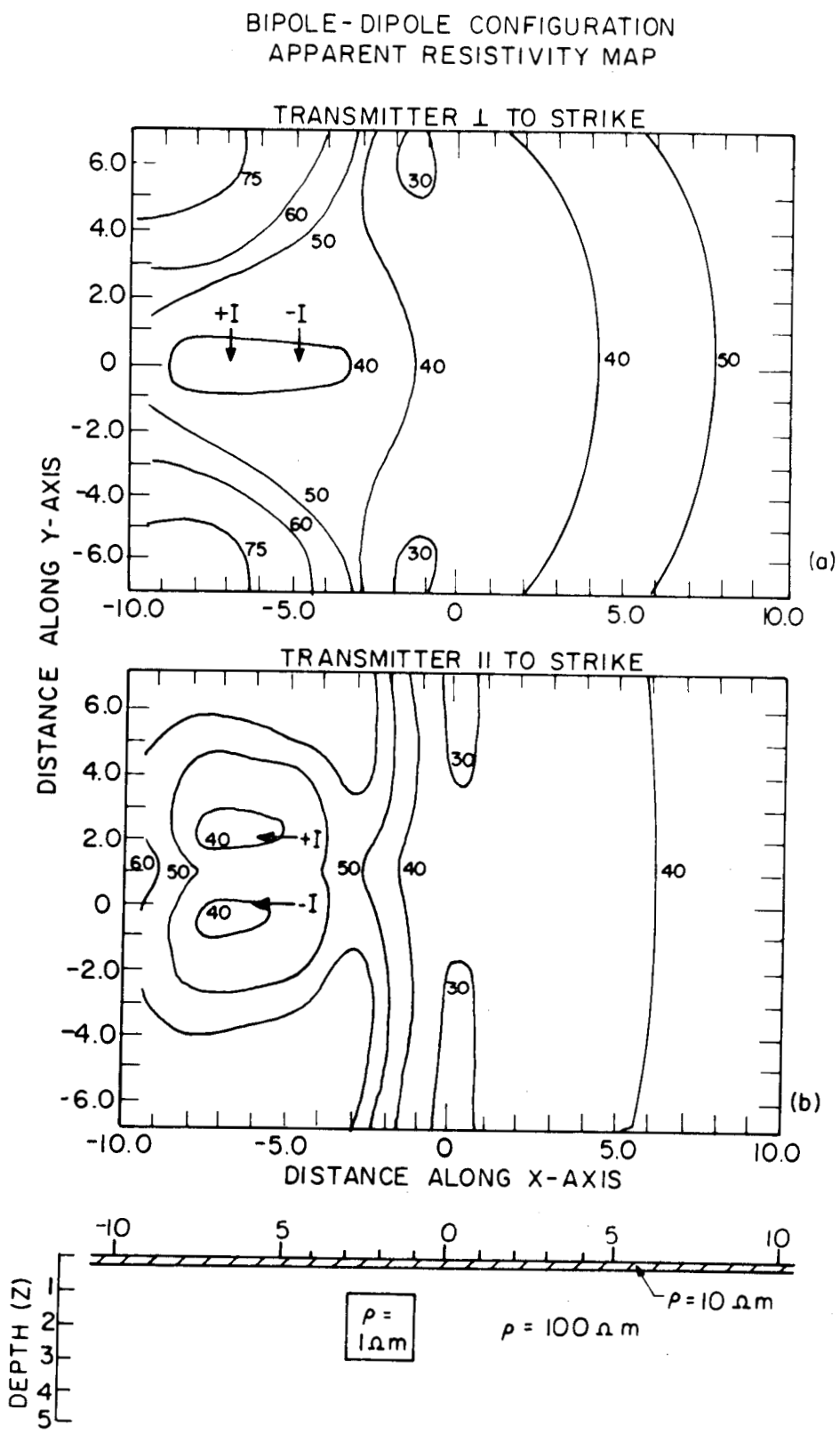
BIPOLE-DIPOLE CONFIGURATION
APPARENT RESISTIVITY MAP
TRANSMITTER ⊥ TO STRIKE
TRANSMITTER ∥ TO STRIKE
DISTANCE ALONG Y-AXIS
DISTANCE ALONG X-AXIS
+I
-I
(a)
(b)
DEPTH (Z)
ρ = 1Ωm
ρ = 10 Ωm
ρ = 100 Ωm

Figure 10

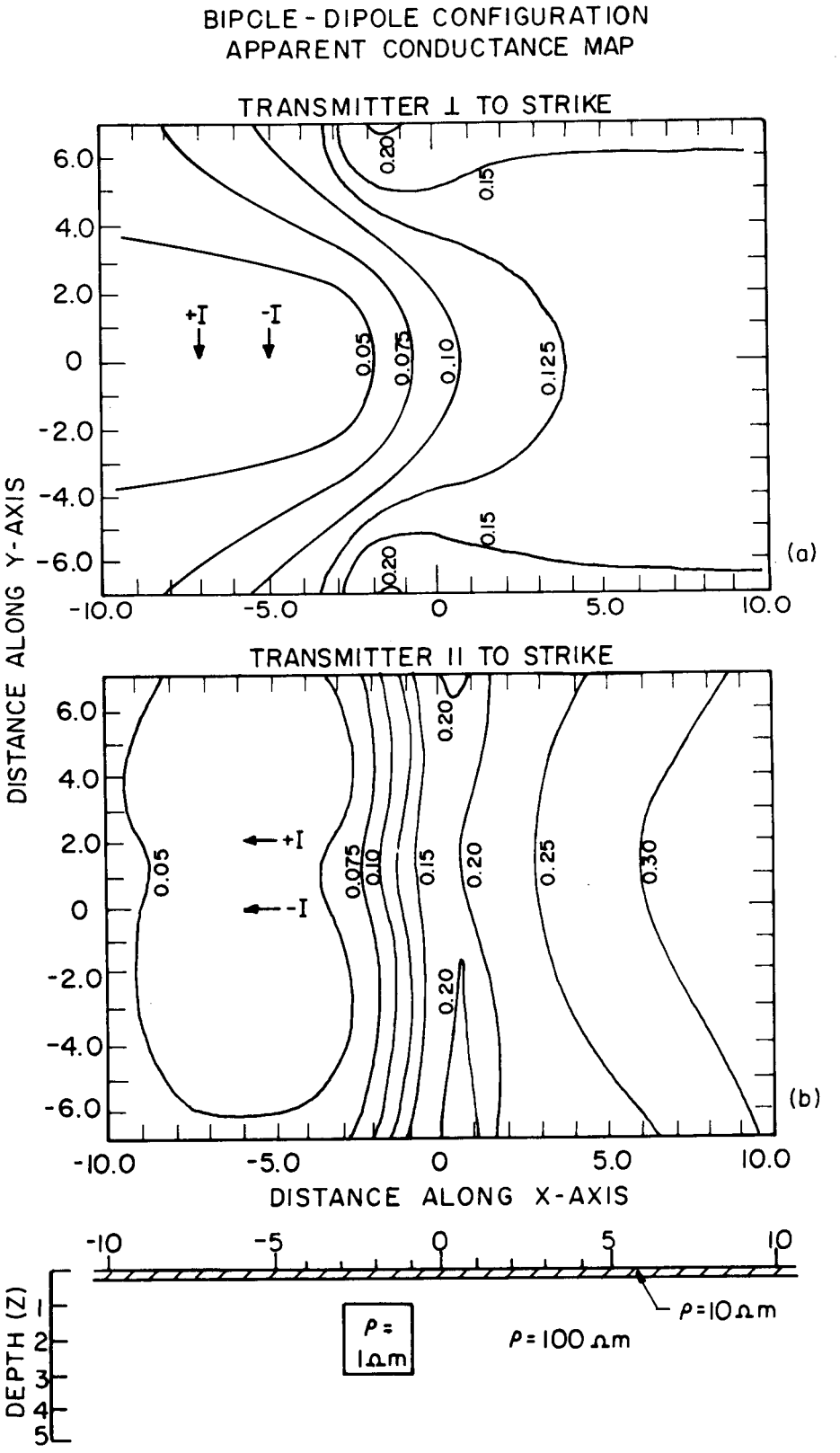
BIPOLE - DIPOLE CONFIGURATION
APPARENT CONDUCTANCE MAP
TRANSMITTER ⊥ TO STRIKE
TRANSMITTER ∥ TO STRIKE
DISTANCE ALONG Y-AXIS
DISTANCE ALONG X-AXIS
+I
-I
0.05
0.075
0.10
0.125
0.15
0.20
0.25
0.30
(a)
(b)
DEPTH (Z)
ρ = 1Ωm
ρ = 100 Ωm
ρ = 10Ωm

Figure 11

DIPOLE - DIPOLE CONFIGURATION OF ELECTRODES
APPARENT RESISTIVITY PSEUDO-SECTION

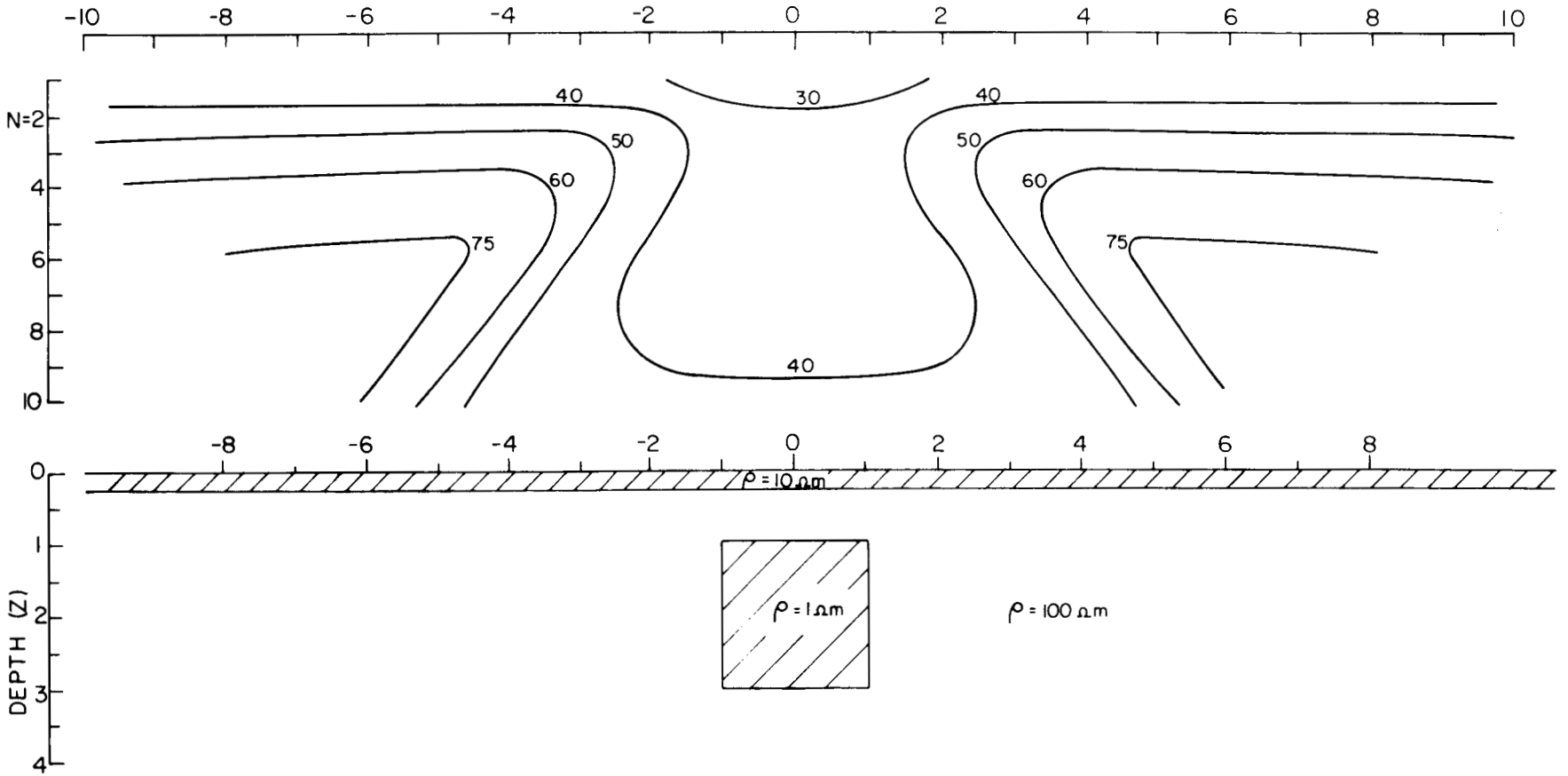

Figure 12

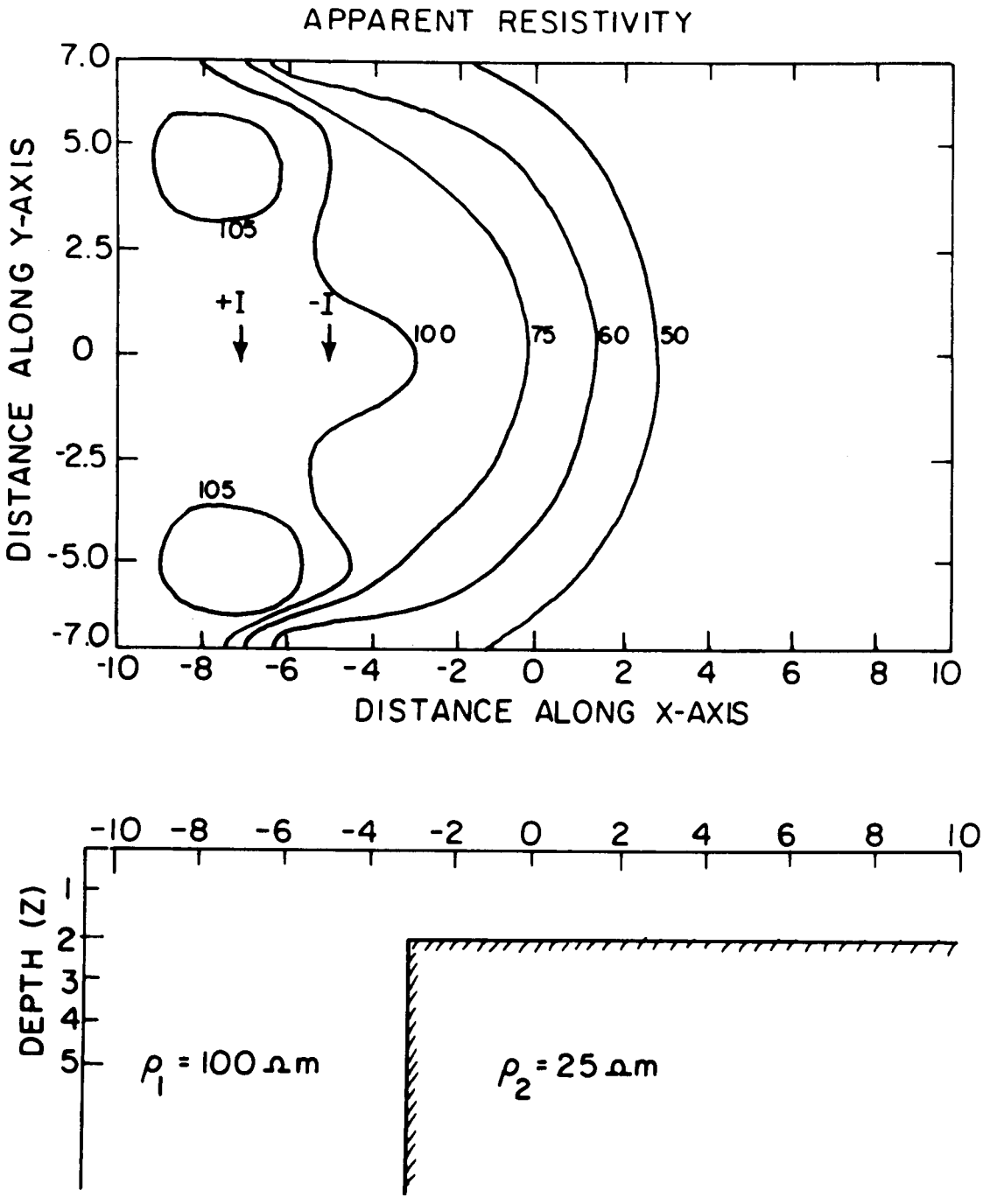
APPARENT RESISTIVITY
DISTANCE ALONG Y-AXIS
7.0
5.0
2.5
0
-2.5
-5.0
-7.0
105
+I
-I
100
75
60
50
105
-10 -8 -6 -4 -2 0 2 4 6 8 10
DISTANCE ALONG X-AXIS
-10 -8 -6 -4 -2 0 2 4 6 8 10
DEPTH (Z)
1
2
3
4
5
ρ1 = 100 Ω m
ρ2 = 25 Ω m

Figure 13

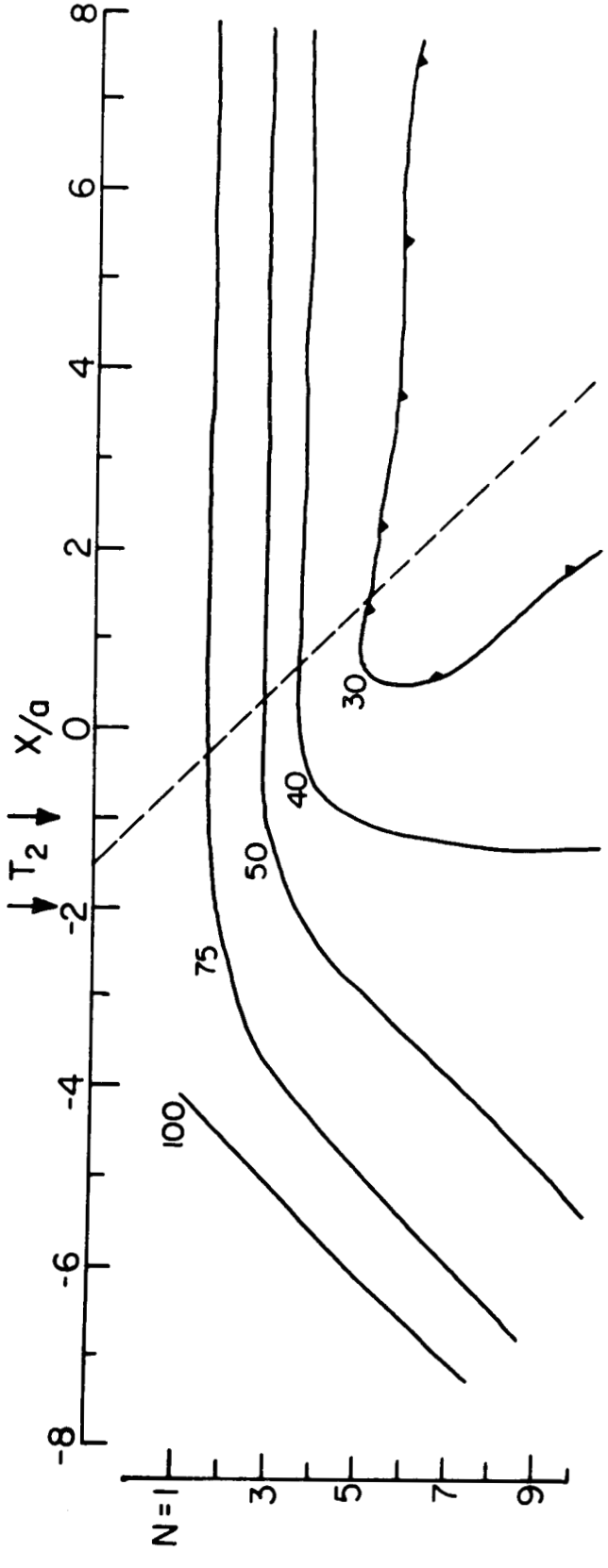

Figure 14

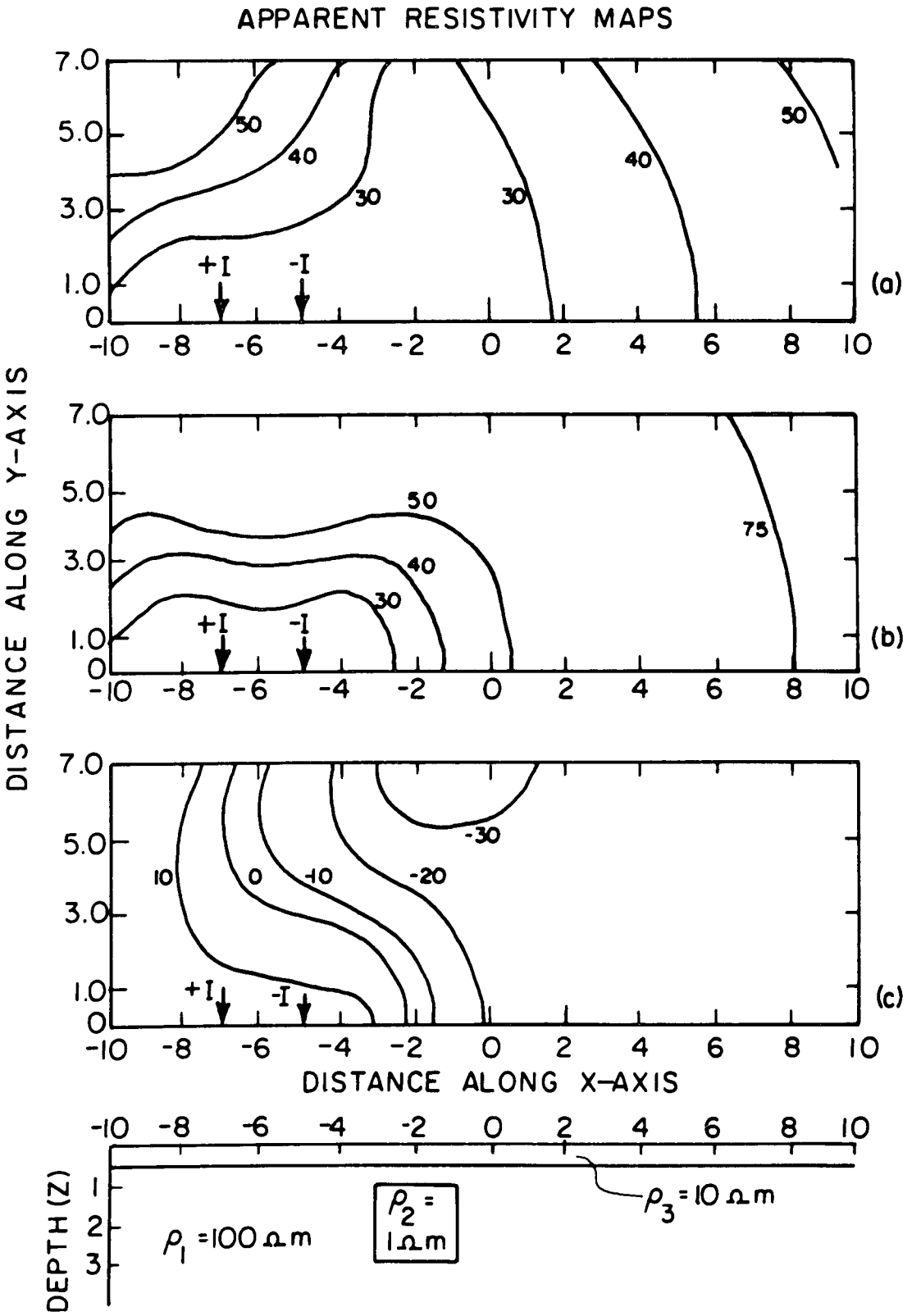
APPARENT RESISTIVITY MAPS
DISTANCE ALONG Y-AXIS
DISTANCE ALONG X-AXIS
DEPTH (Z)
7.0
5.0
3.0
1.0
0
-10 -8 -6 -4 -2 0 2 4 6 8 10
50
40
30
+I
-I
(a)
75
(b)
-30
10
-20
(c)
ρ_1 = 100 Ω m
ρ_2 = 1 Ω m
ρ_3 = 10 Ω m

Figure 15

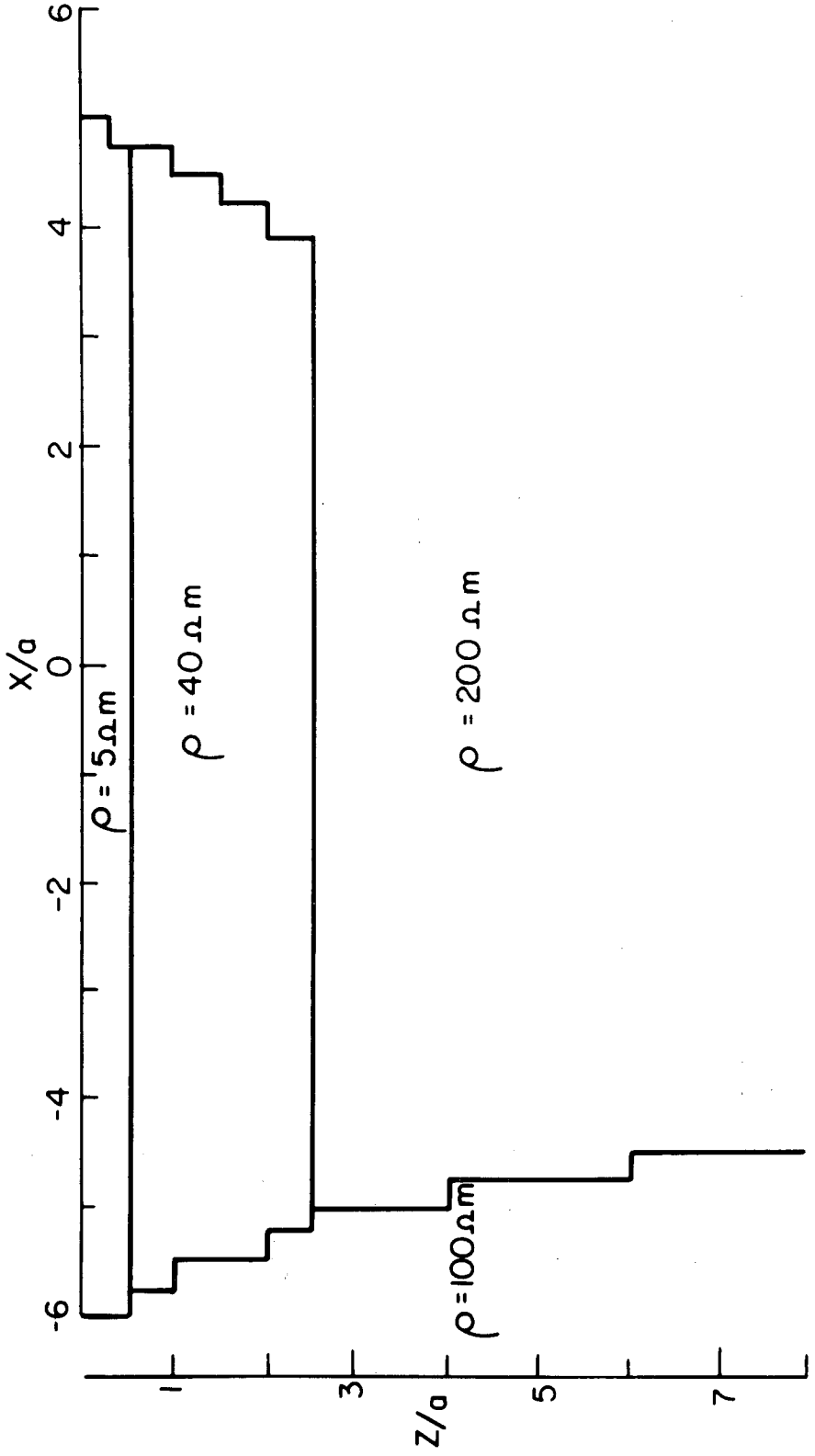

Figure 16

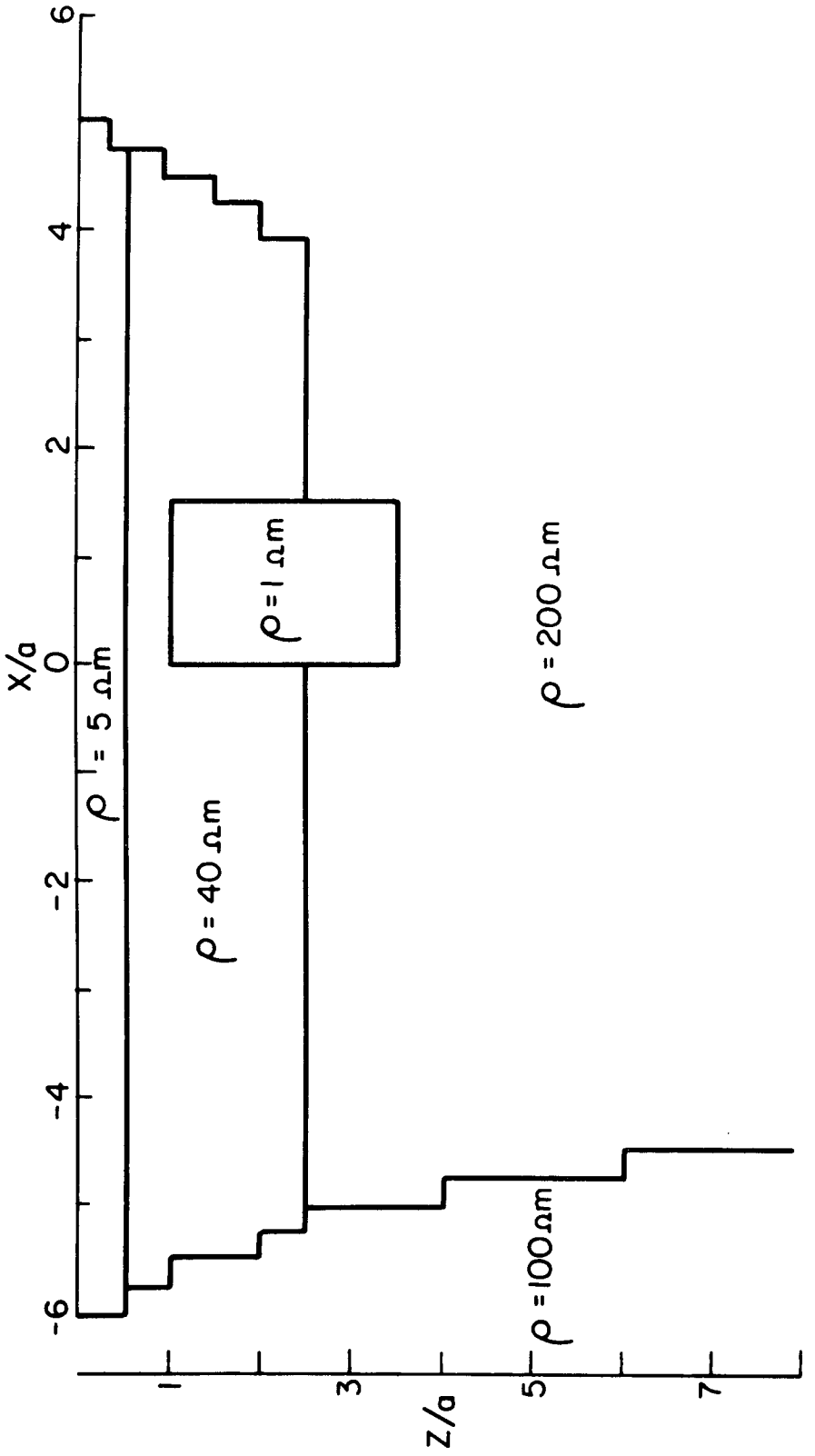

Figure 17

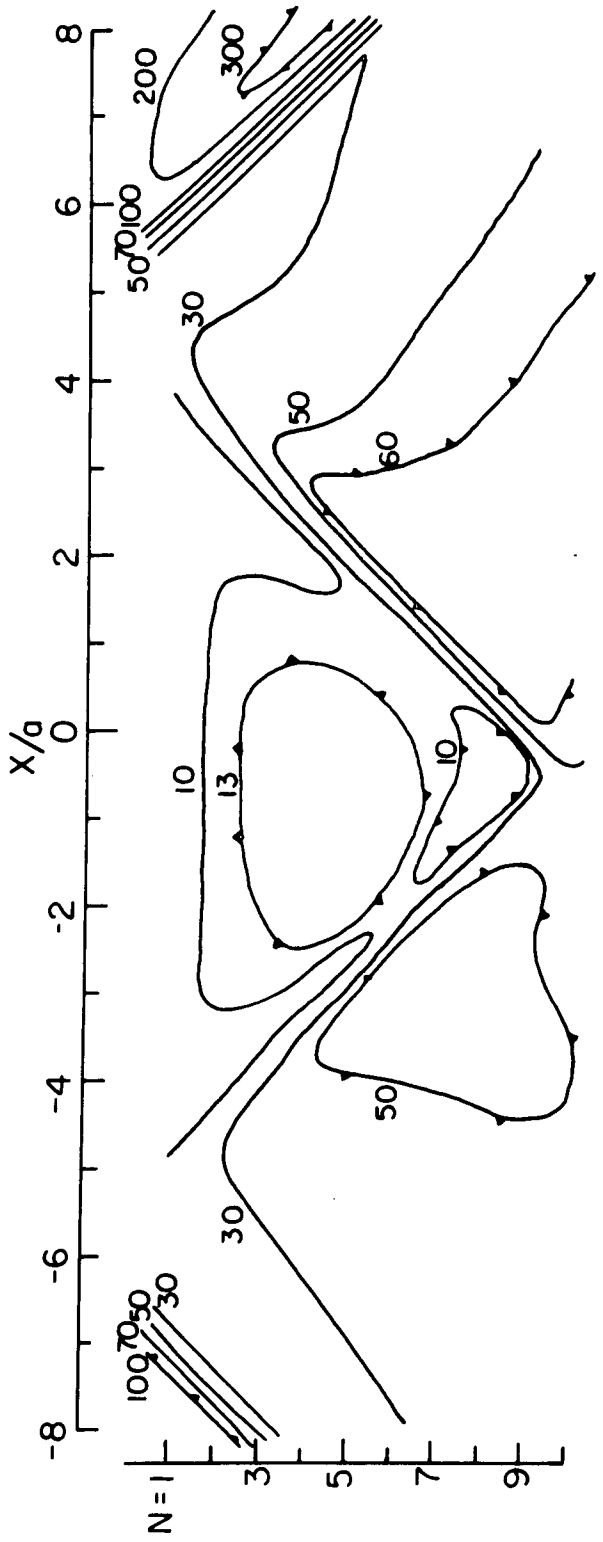
X/a
8
6
4
2
0
-2
-4
-6
-8
N=1
3
5
7
9
200
300
100
70
50
30
50
60
10
13
10
50
30
100
70
50
30

Figure 18

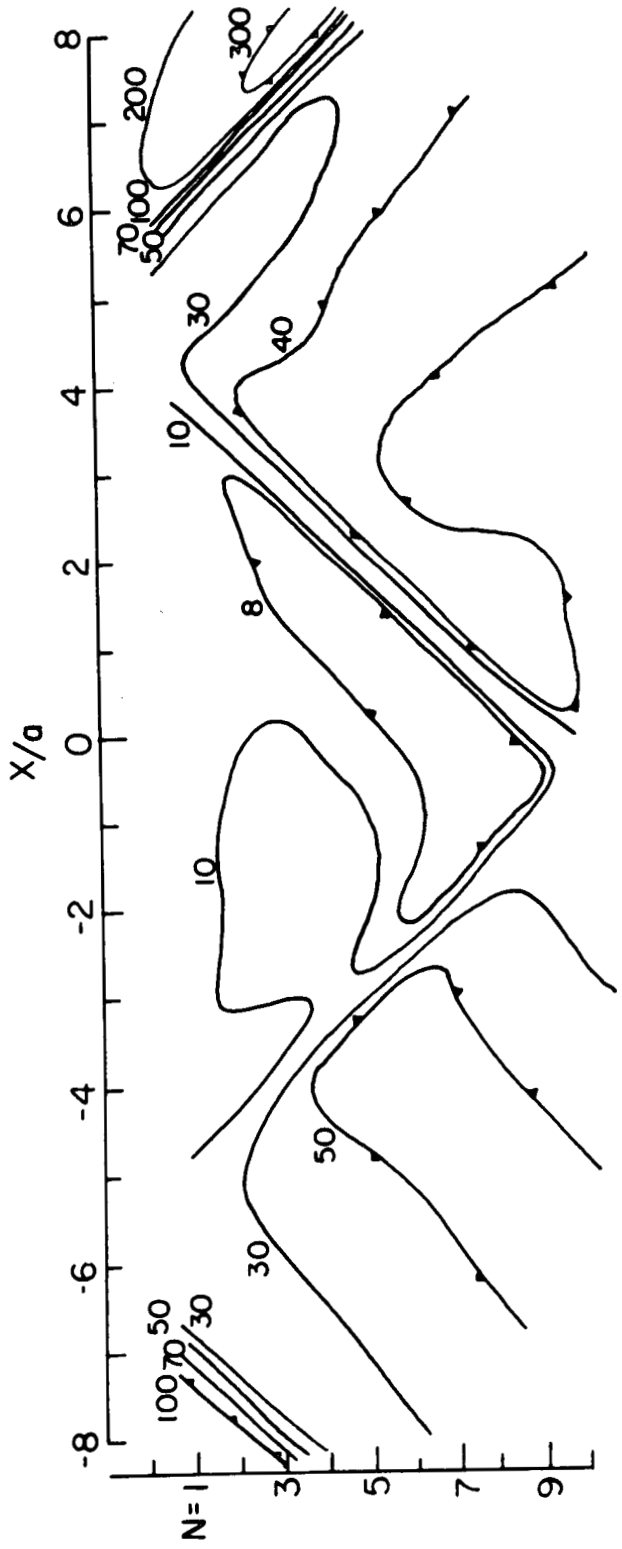
X/a
8
6
4
2
0
-2
-4
-6
-8
N= 1
3
5
7
9
300
200
100
70
50
30
40
10
8
10
30
50
30
50
70
100

Figure 19

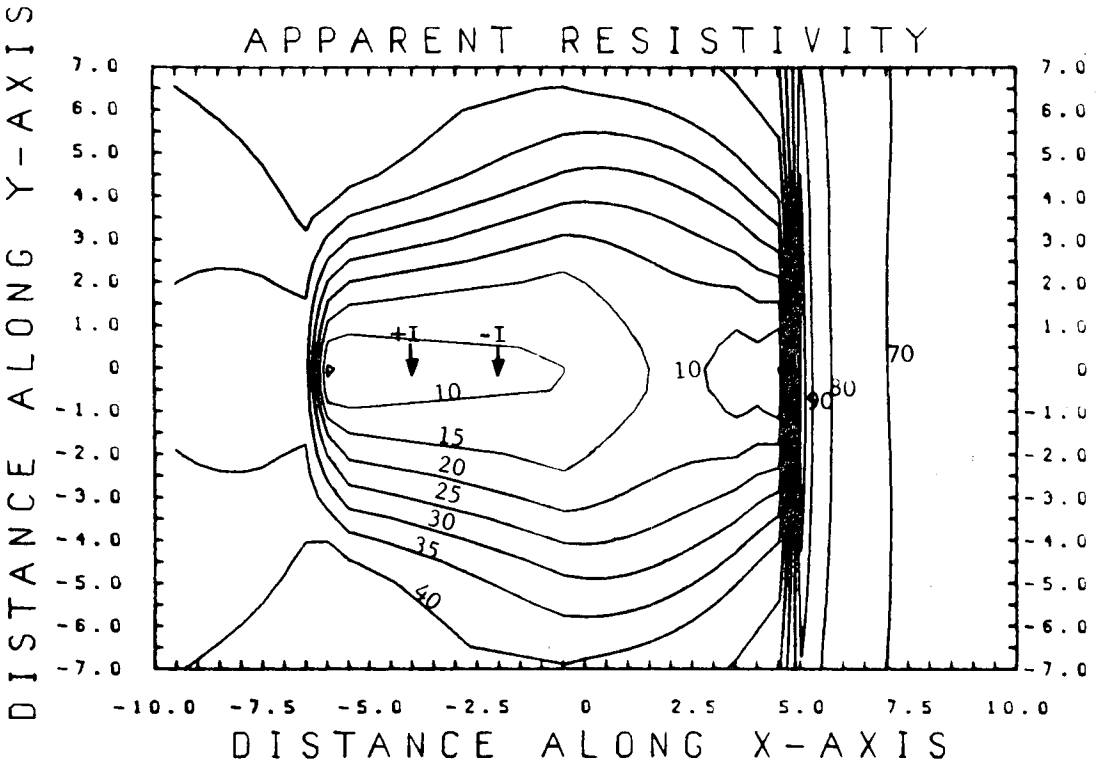
APPARENT RESISTIVITY
DISTANCE ALONG Y-AXIS
DISTANCE ALONG X-AXIS
+I
-I
10
15
20
25
30
35
40
10
70
80
90
7.0
6.0
5.0
4.0
3.0
2.0
1.0
0
-1.0
-2.0
-3.0
-4.0
-5.0
-6.0
-7.0
-10.0
-7.5
-5.0
-2.5
0
2.5
5.0
7.5
10.0

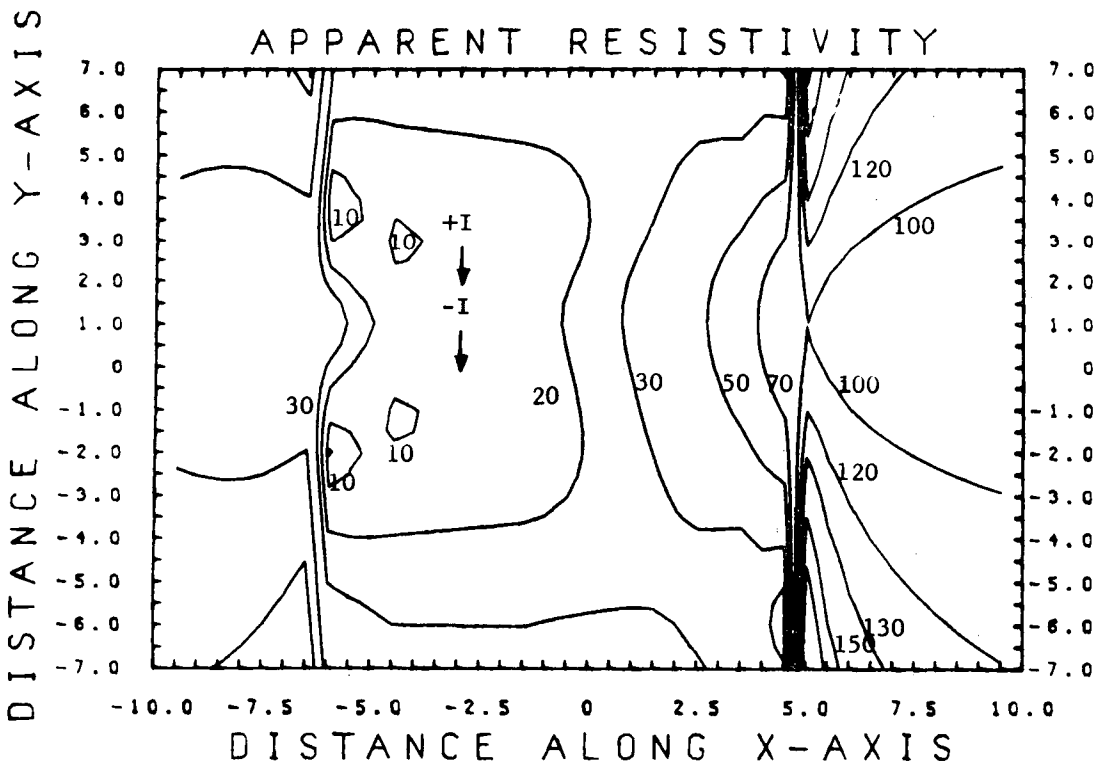
APPARENT RESISTIVITY
DISTANCE ALONG Y-AXIS
DISTANCE ALONG X-AXIS
+I
-I
10
10
10
10
10
20
30
30
50
70
100
100
120
120
130
150
7.0
6.0
5.0
4.0
3.0
2.0
1.0
0
-1.0
-2.0
-3.0
-4.0
-5.0
-6.0
-7.0
-10.0
-7.5
-5.0
-2.5
0
2.5
5.0
7.5
10.0

Figure 20

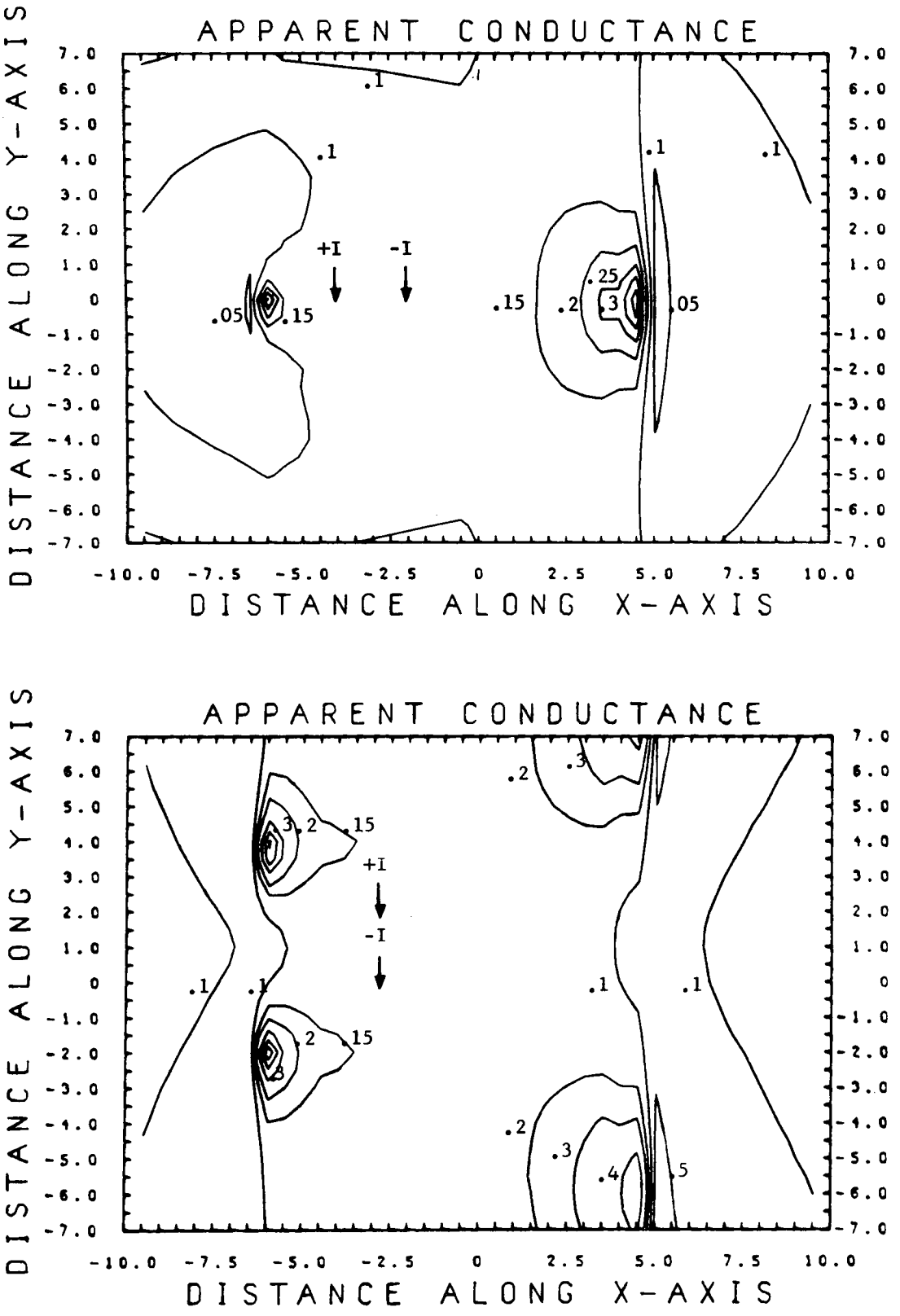
APPARENT CONDUCTANCE
DISTANCE ALONG Y-AXIS
DISTANCE ALONG X-AXIS
+I
-I
.1
.05
.15
.2
.25
.3
.4
.5
7.0
6.0
5.0
4.0
3.0
2.0
1.0
0
-1.0
-2.0
-3.0
-4.0
-5.0
-6.0
-7.0
-10.0
-7.5
-5.0
-2.5
2.5
5.0
7.5
10.0

Figure 21

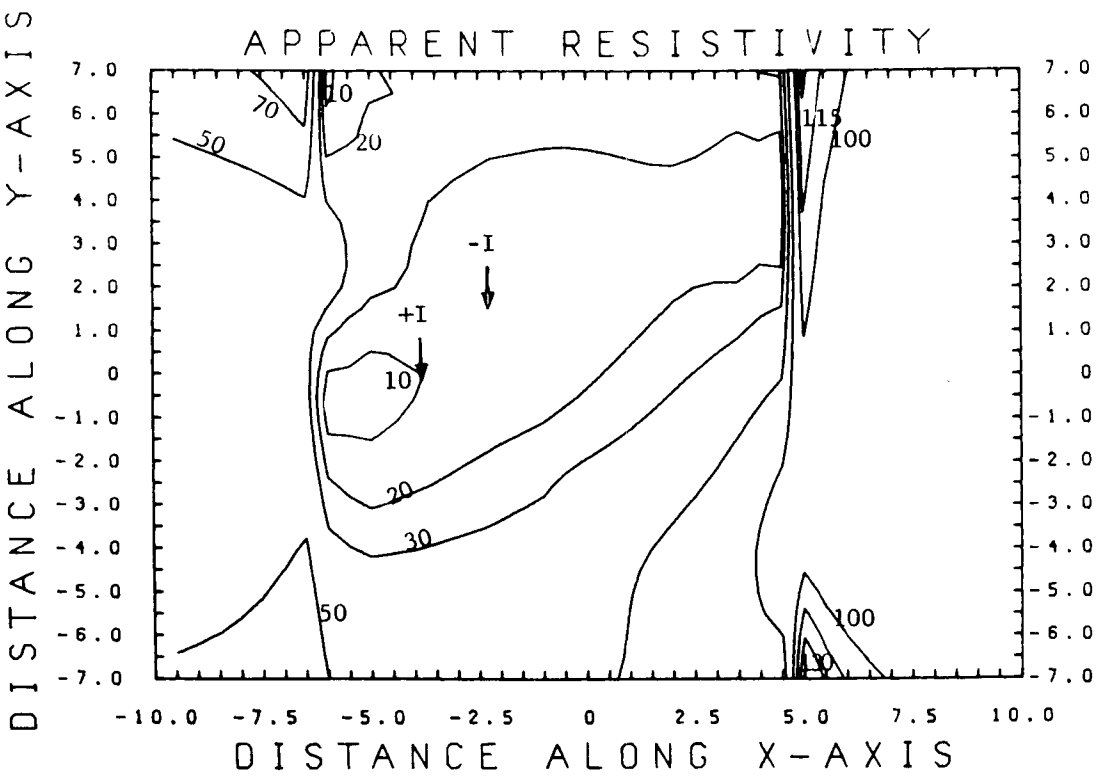
APPARENT RESISTIVITY
DISTANCE ALONG Y-AXIS
DISTANCE ALONG X-AXIS
+I
-I
10
20
30
50
70
100
115
7.0
6.0
5.0
4.0
3.0
2.0
1.0
0
-1.0
-2.0
-3.0
-4.0
-5.0
-6.0
-7.0
-10.0
-7.5
-5.0
-2.5
2.5
5.0
7.5
10.0

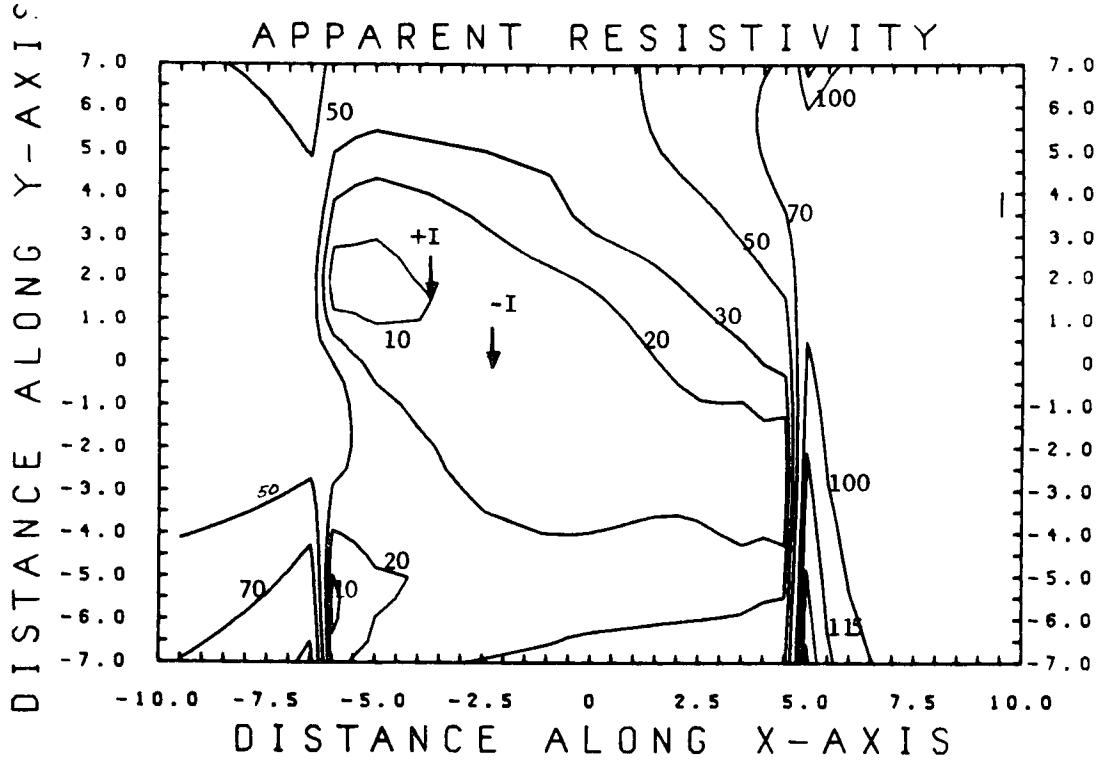
APPARENT RESISTIVITY
DISTANCE ALONG Y-AXIS
DISTANCE ALONG X-AXIS
+I
-I
10
20
30
50
70
100
115
7.0
6.0
5.0
4.0
3.0
2.0
1.0
0
-1.0
-2.0
-3.0
-4.0
-5.0
-6.0
-7.0
-10.0
-7.5
-5.0
-2.5
2.5
5.0
7.5
10.0

Figure 22

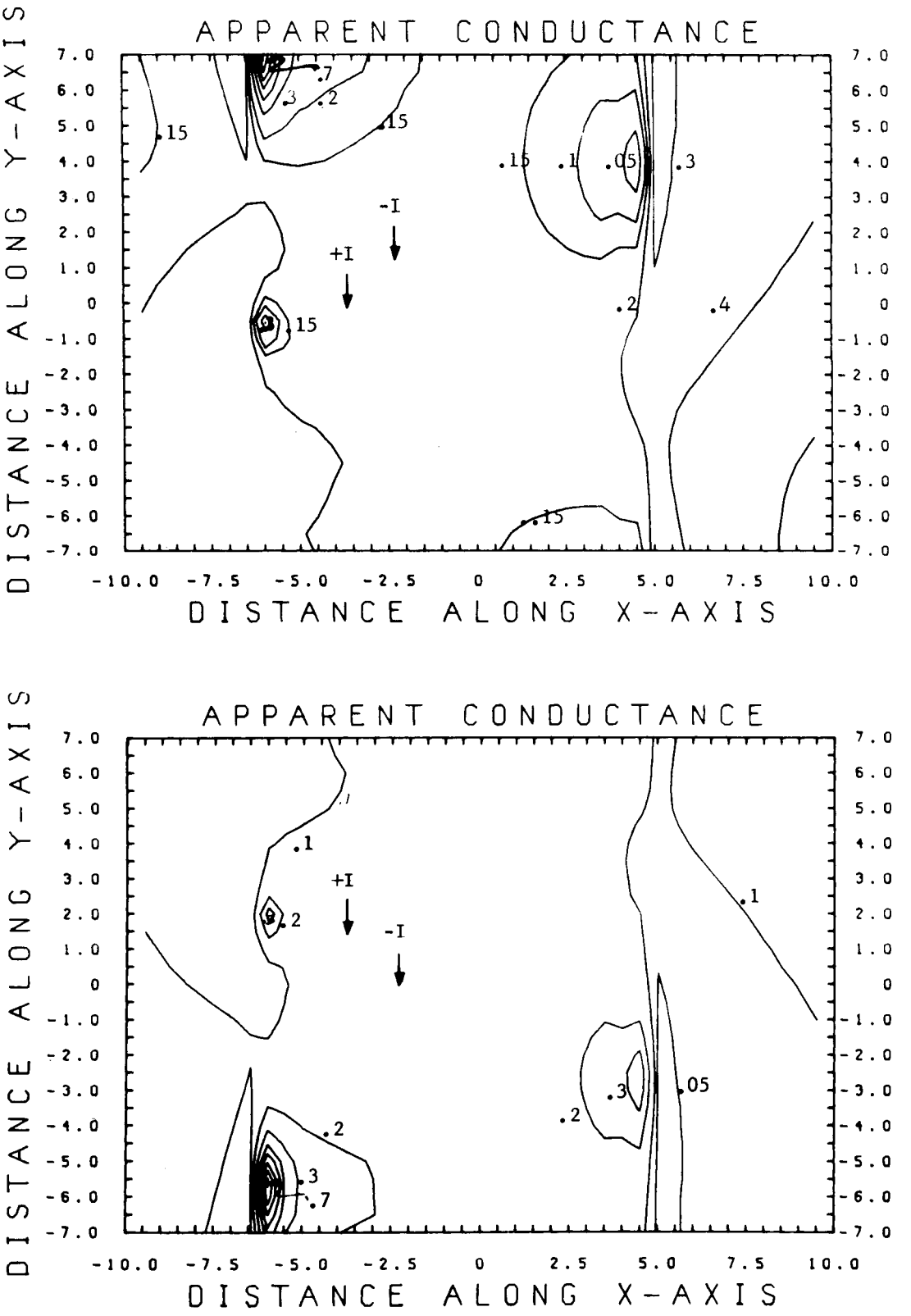
APPARENT CONDUCTANCE
DISTANCE ALONG Y-AXIS
DISTANCE ALONG X-AXIS
+I
-I
.7
.3
.2
.15
.1
.05
.4
7.0
6.0
5.0
4.0
3.0
2.0
1.0
0
-1.0
-2.0
-3.0
-4.0
-5.0
-6.0
-7.0
-10.0
-7.5
-5.0
-2.5
2.5
5.0
7.5
10.0

Figure 23

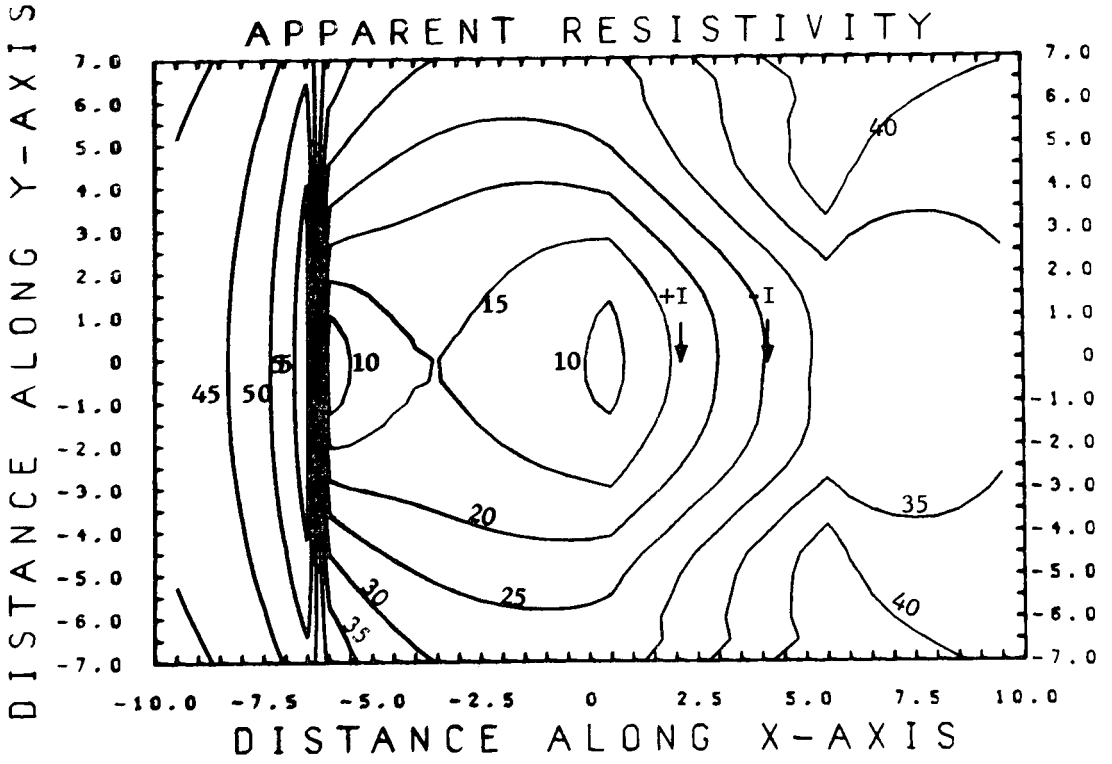
APPARENT RESISTIVITY
DISTANCE ALONG Y-AXIS
DISTANCE ALONG X-AXIS
7.0
6.0
5.0
4.0
3.0
2.0
1.0
0
-1.0
-2.0
-3.0
-4.0
-5.0
-6.0
-7.0
-10.0
-7.5
-5.0
-2.5
0
2.5
5.0
7.5
10.0
40
15
+I
+I
10
10
45
50
35
20
30
25
35
40

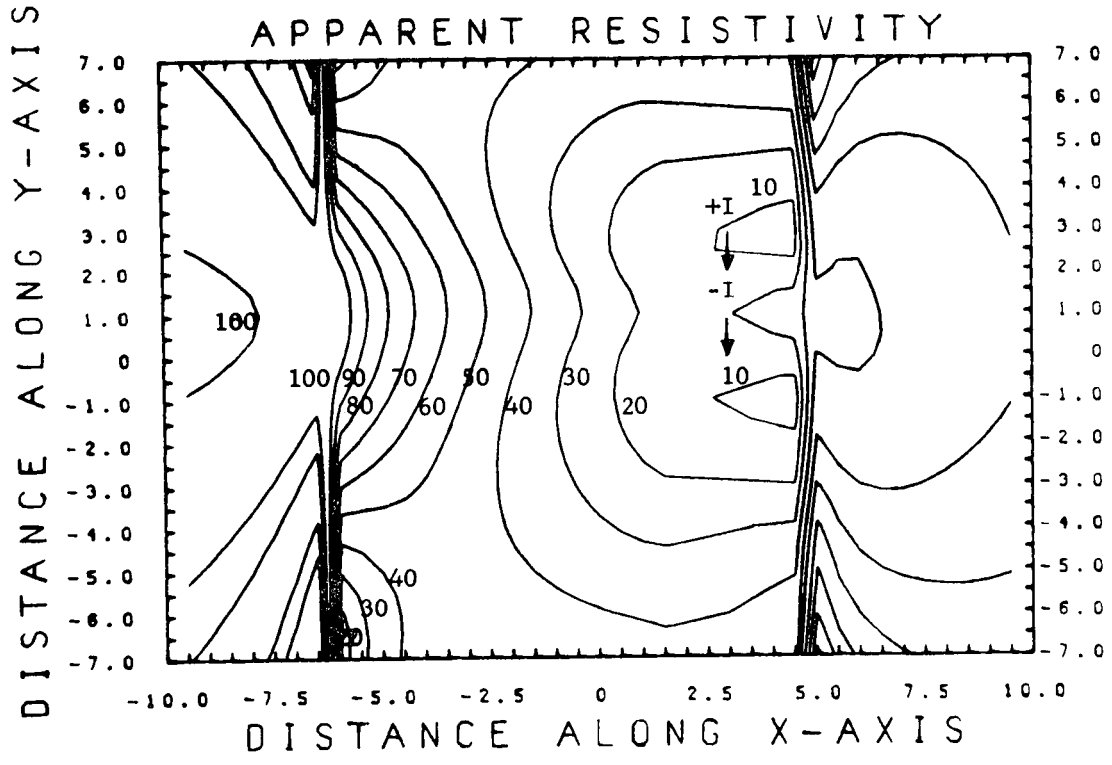
APPARENT RESISTIVITY
DISTANCE ALONG Y-AXIS
DISTANCE ALONG X-AXIS
7.0
6.0
5.0
4.0
3.0
2.0
1.0
0
-1.0
-2.0
-3.0
-4.0
-5.0
-6.0
-7.0
-10.0
-7.5
-5.0
-2.5
0
2.5
5.0
7.5
10.0
+I
10
-I
10
100
100
90
80
70
60
50
40
30
20
40
30

Figure 24

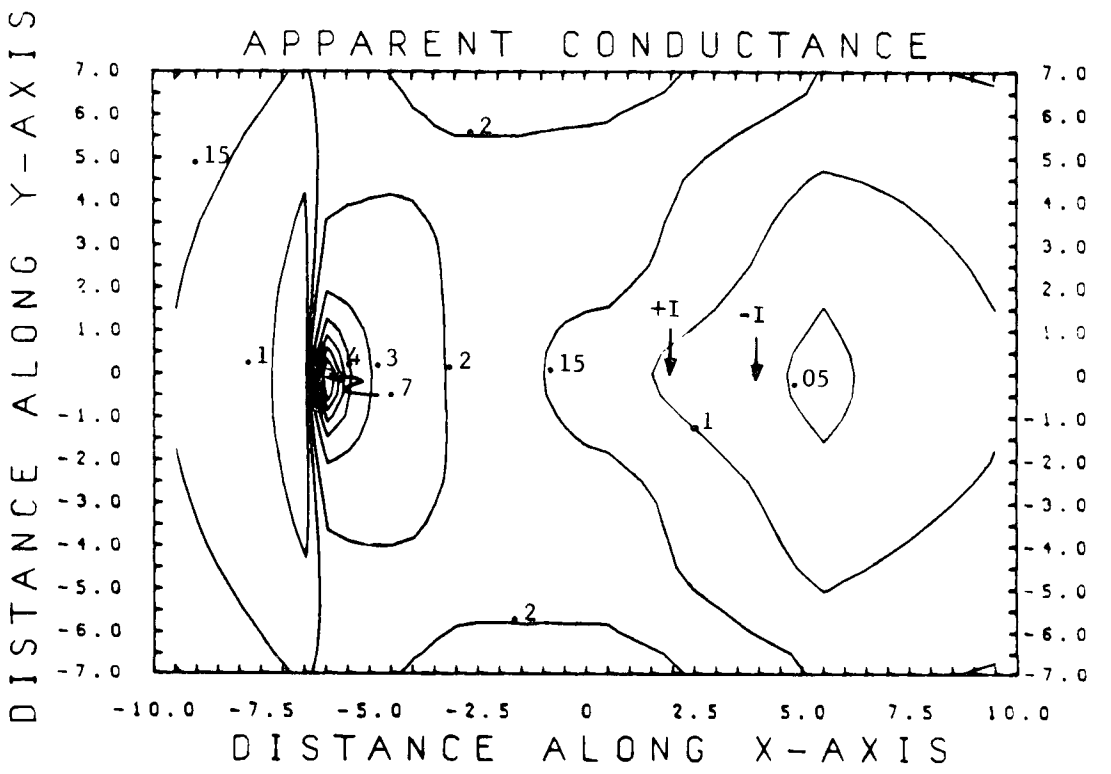
APPARENT CONDUCTANCE
DISTANCE ALONG Y-AXIS
DISTANCE ALONG X-AXIS
+I
-I
.15
.2
.1
.3
.7
.05
7.0
6.0
5.0
4.0
3.0
2.0
1.0
0
-1.0
-2.0
-3.0
-4.0
-5.0
-6.0
-7.0
-10.0
-7.5
-5.0
-2.5
2.5
5.0
7.5
10.0

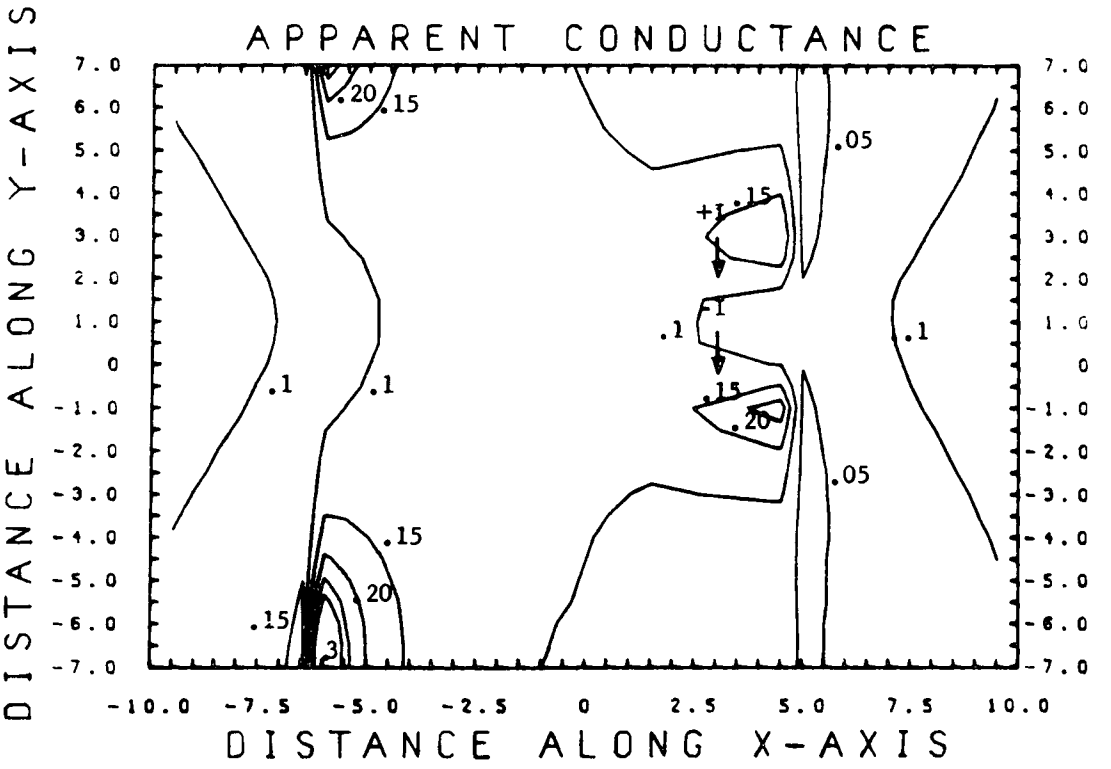
APPARENT CONDUCTANCE
DISTANCE ALONG Y-AXIS
DISTANCE ALONG X-AXIS
+I
-I
.20
.15
.05
.1
.3
7.0
6.0
5.0
4.0
3.0
2.0
1.0
0
-1.0
-2.0
-3.0
-4.0
-5.0
-6.0
-7.0
-10.0
-7.5
-5.0
-2.5
2.5
5.0
7.5
10.0

Figure 25

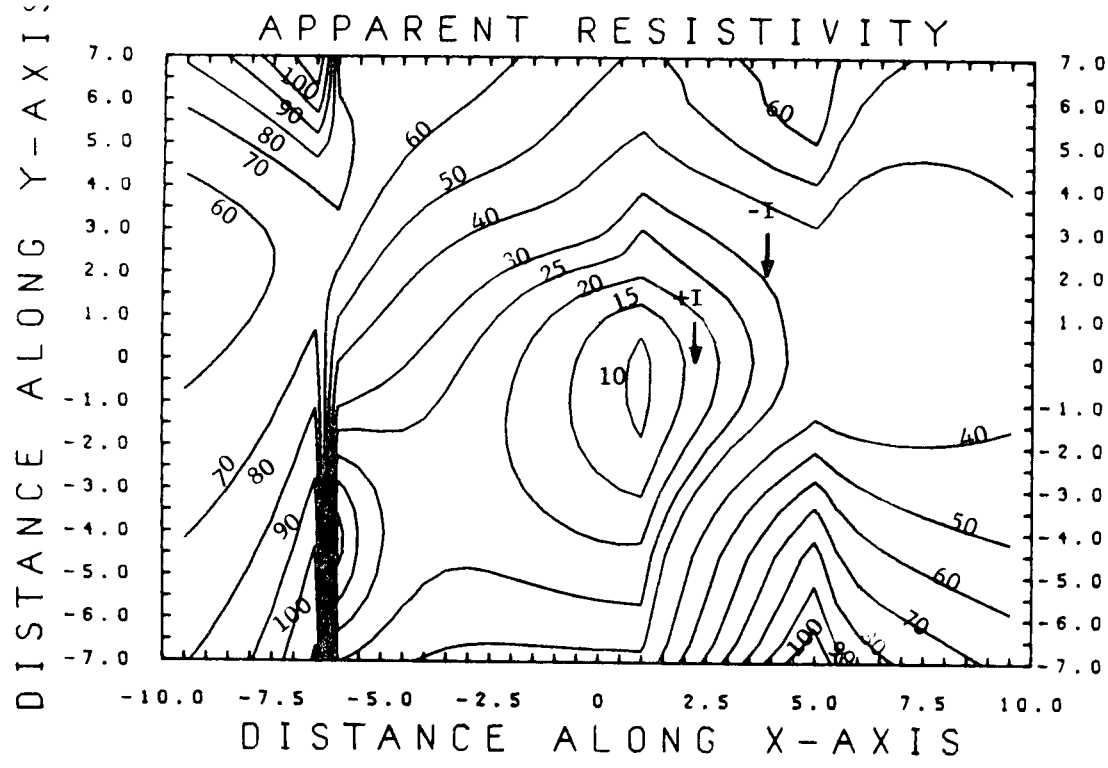
APPARENT RESISTIVITY
DISTANCE ALONG Y-AXIS
DISTANCE ALONG X-AXIS
-I
+I
10
15
20
25
30
40
50
60
70
80
90
100
7.0
6.0
5.0
4.0
3.0
2.0
1.0
0
-1.0
-2.0
-3.0
-4.0
-5.0
-6.0
-7.0
-10.0
-7.5
-5.0
-2.5
2.5
5.0
7.5
10.0

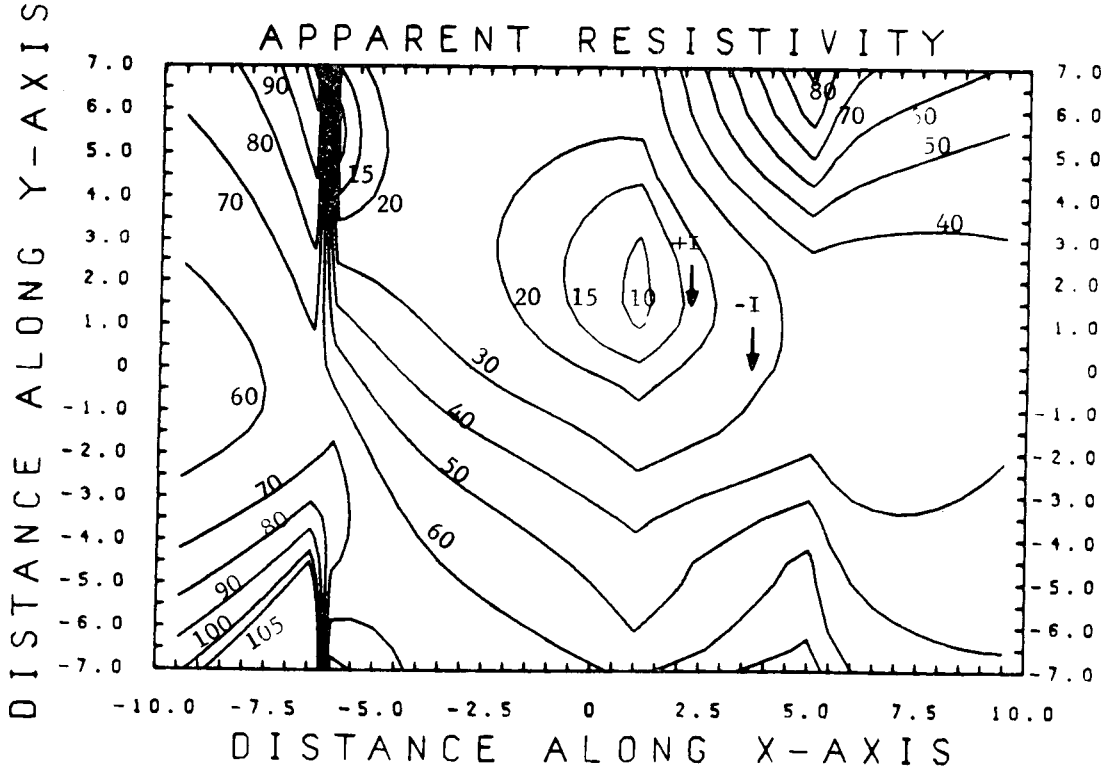
APPARENT RESISTIVITY
DISTANCE ALONG Y-AXIS
DISTANCE ALONG X-AXIS
-I
+I
10
15
20
30
40
50
60
70
80
90
100
105
7.0
6.0
5.0
4.0
3.0
2.0
1.0
0
-1.0
-2.0
-3.0
-4.0
-5.0
-6.0
-7.0
-10.0
-7.5
-5.0
-2.5
2.5
5.0
7.5
10.0

Figure 26

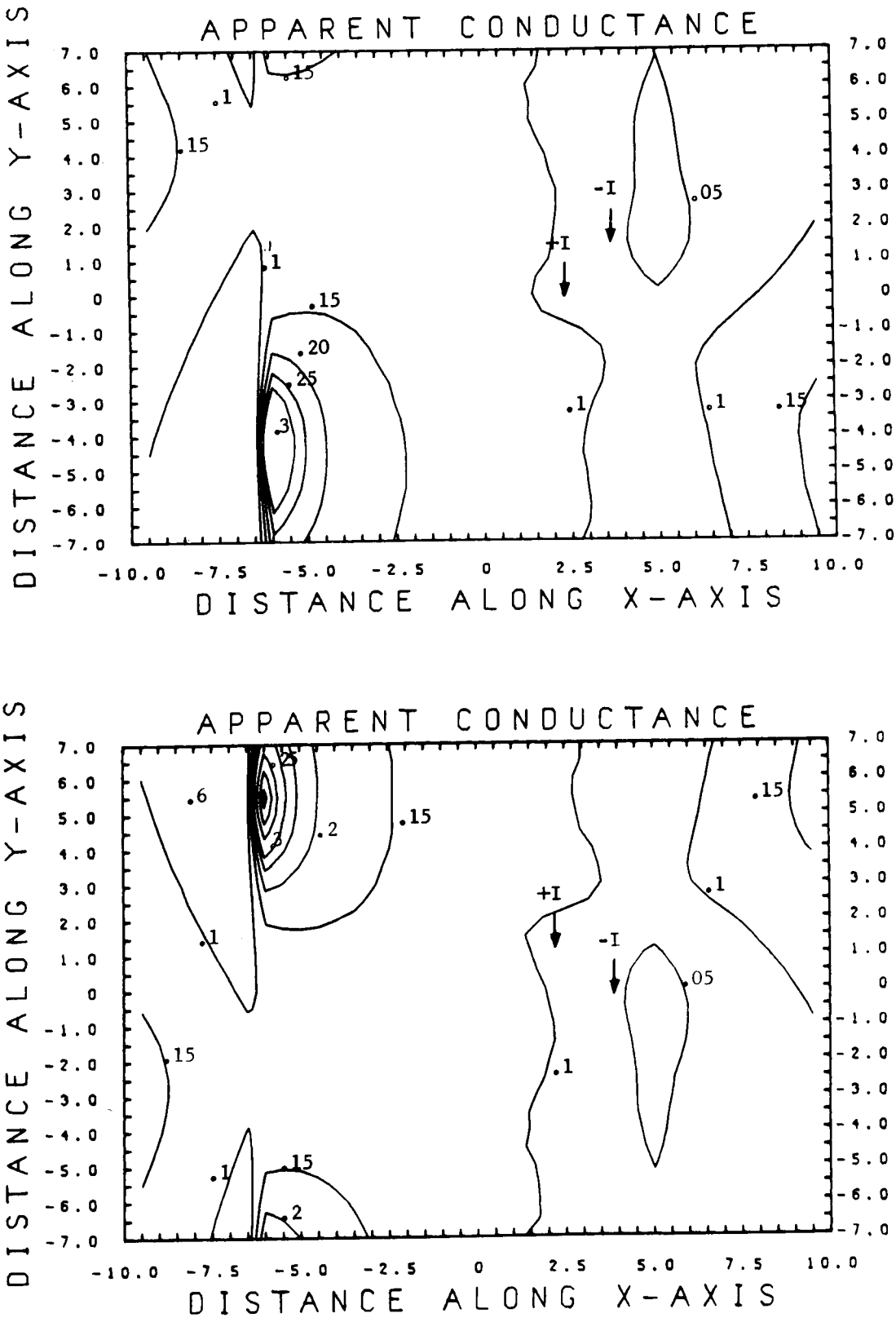
APPARENT CONDUCTANCE
DISTANCE ALONG Y-AXIS
DISTANCE ALONG X-AXIS
7.0
6.0
5.0
4.0
3.0
2.0
1.0
0
-1.0
-2.0
-3.0
-4.0
-5.0
-6.0
-7.0
-10.0
-7.5
-5.0
-2.5
2.5
5.0
7.5
10.0
.1
.15
.05
.20
.25
.3
.6
.2
-I
+I
APPARENT CONDUCTANCE
DISTANCE ALONG Y-AXIS
DISTANCE ALONG X-AXIS

Figure 27

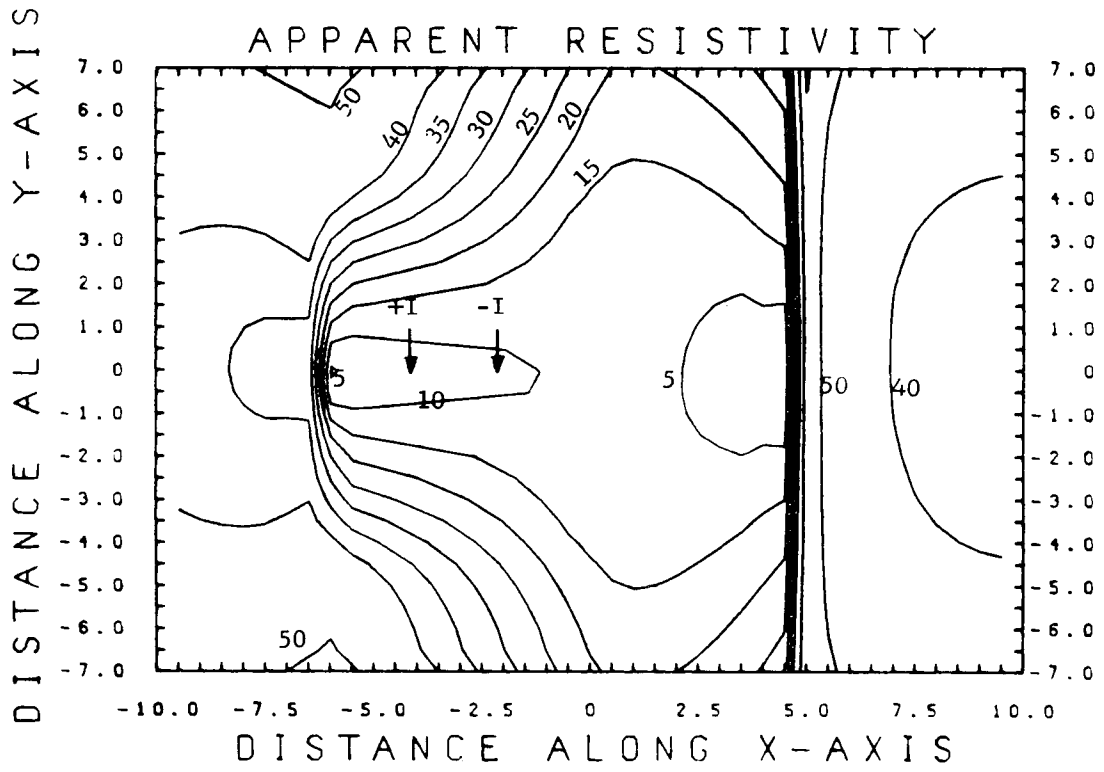
APPARENT RESISTIVITY
DISTANCE ALONG Y-AXIS
DISTANCE ALONG X-AXIS
+I
-I
50
40
35
30
25
20
15
10
5
60
70
80

Figure 28

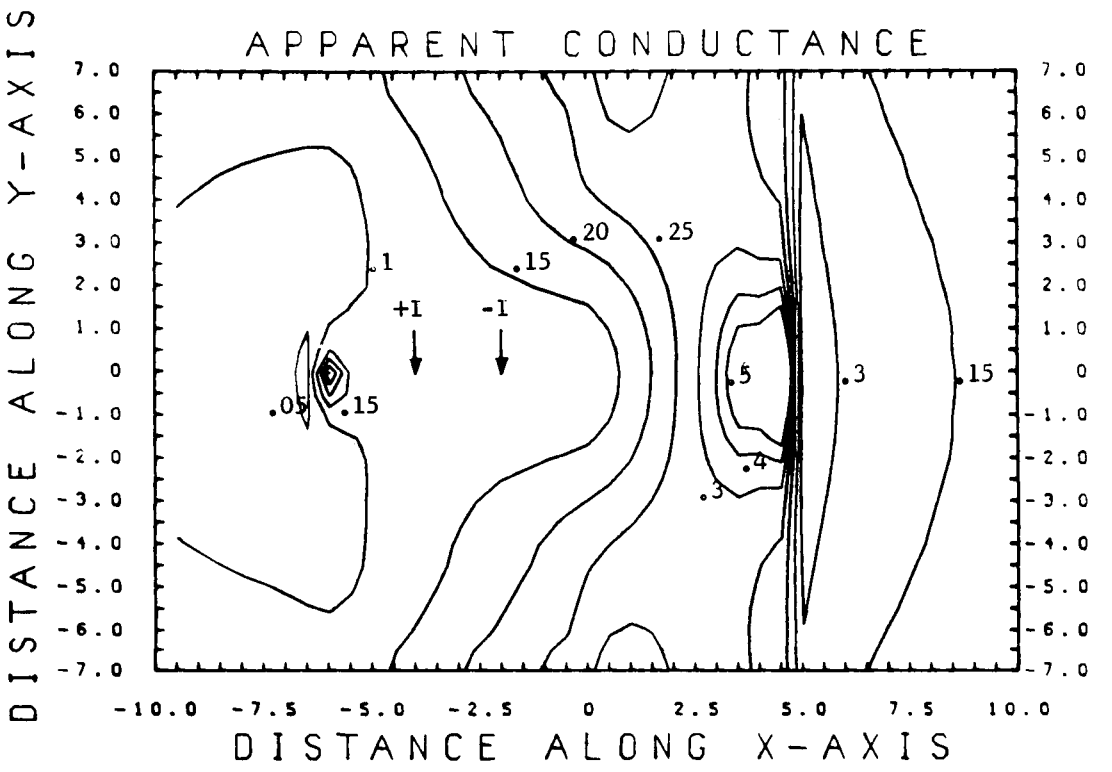
APPARENT CONDUCTANCE
DISTANCE ALONG Y-AXIS
DISTANCE ALONG X-AXIS
+I
-I
.05
.1
.15
.20
.25
.3
.4
.5
.15
7.0
6.0
5.0
4.0
3.0
2.0
1.0
0
-1.0
-2.0
-3.0
-4.0
-5.0
-6.0
-7.0
-10.0
-7.5
-5.0
-2.5
0
2.5
5.0
7.5
10.0

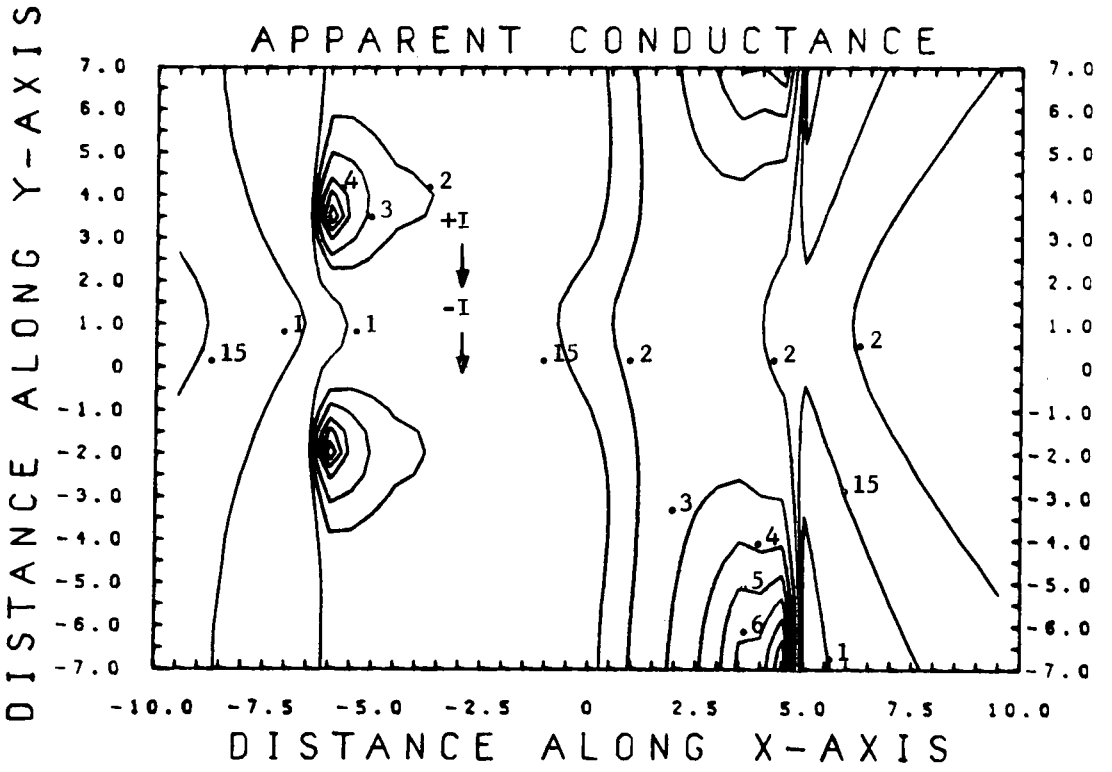
APPARENT CONDUCTANCE
DISTANCE ALONG Y-AXIS
DISTANCE ALONG X-AXIS
+I
-I
.1
.15
.2
.3
.4
.5
.6
.15
7.0
6.0
5.0
4.0
3.0
2.0
1.0
0
-1.0
-2.0
-3.0
-4.0
-5.0
-6.0
-7.0
-10.0
-7.5
-5.0
-2.5
0
2.5
5.0
7.5
10.0

Figure 29

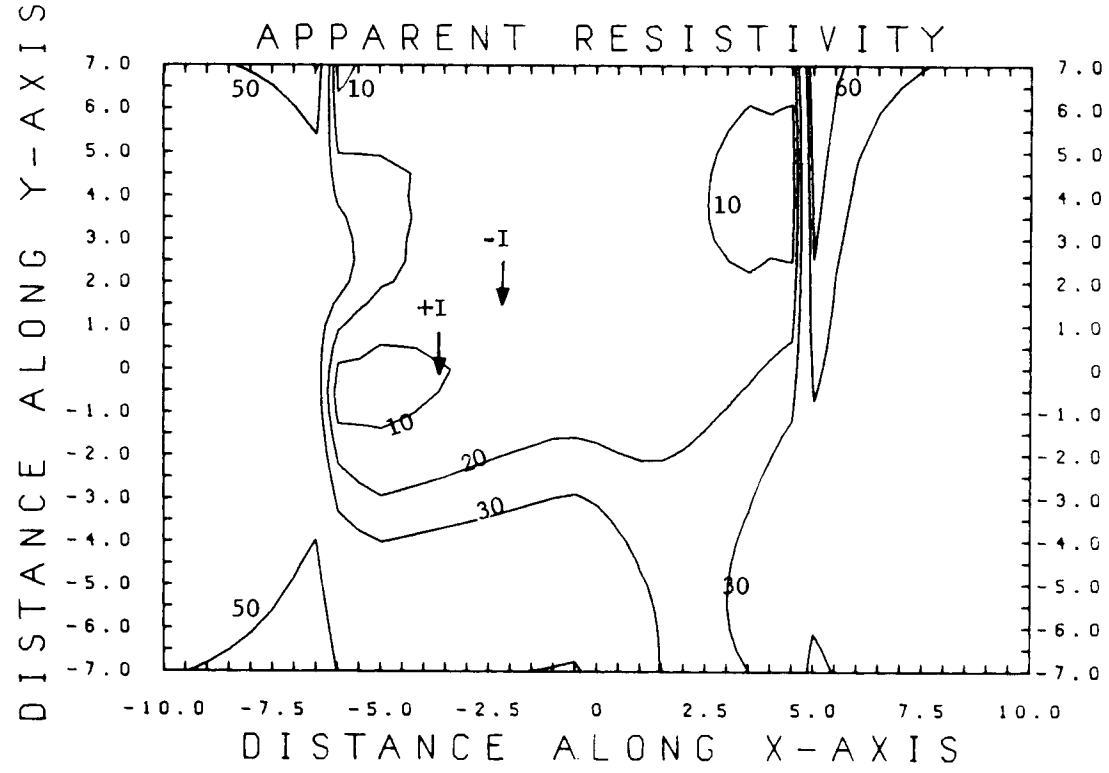
APPARENT RESISTIVITY
DISTANCE ALONG Y-AXIS
DISTANCE ALONG X-AXIS
+I
-I
50
10
60
10
10
20
30
30
50
7.0
6.0
5.0
4.0
3.0
2.0
1.0
0
-1.0
-2.0
-3.0
-4.0
-5.0
-6.0
-7.0
-10.0
-7.5
-5.0
-2.5
0
2.5
5.0
7.5
10.0

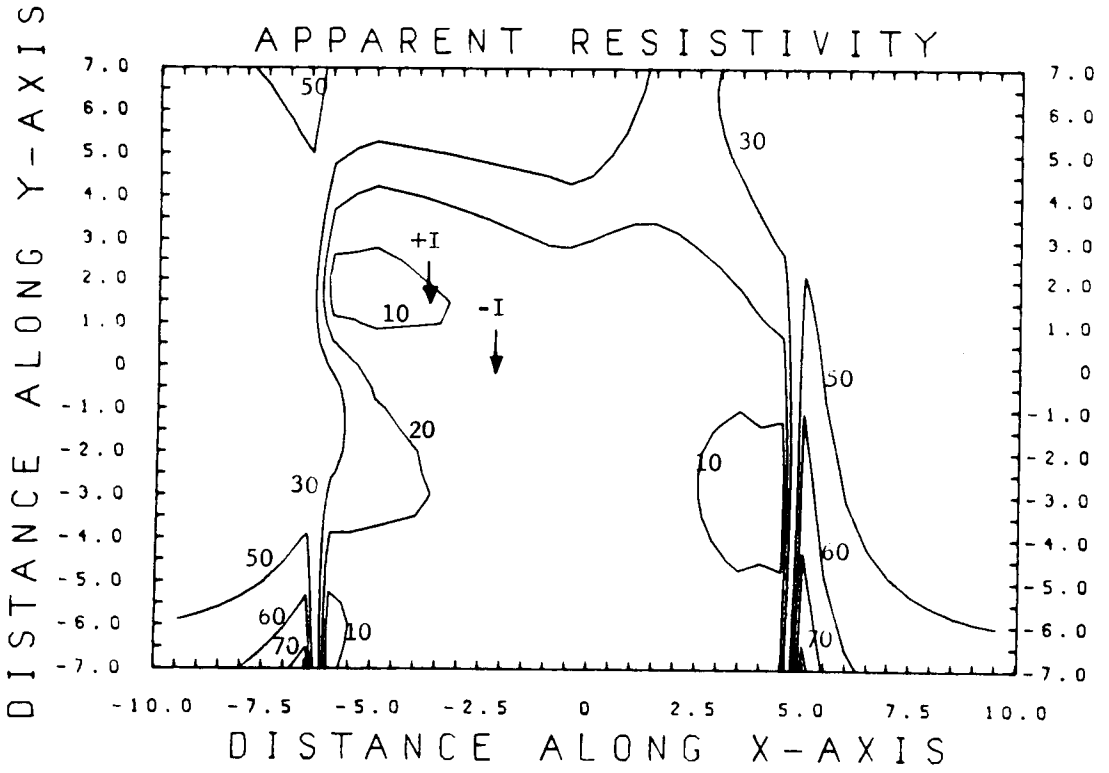
APPARENT RESISTIVITY
DISTANCE ALONG Y-AXIS
DISTANCE ALONG X-AXIS
+I
-I
50
30
10
50
20
10
30
50
60
10
70
60
70
7.0
6.0
5.0
4.0
3.0
2.0
1.0
0
-1.0
-2.0
-3.0
-4.0
-5.0
-6.0
-7.0
-10.0
-7.5
-5.0
-2.5
0
2.5
5.0
7.5
10.0

Figure 30

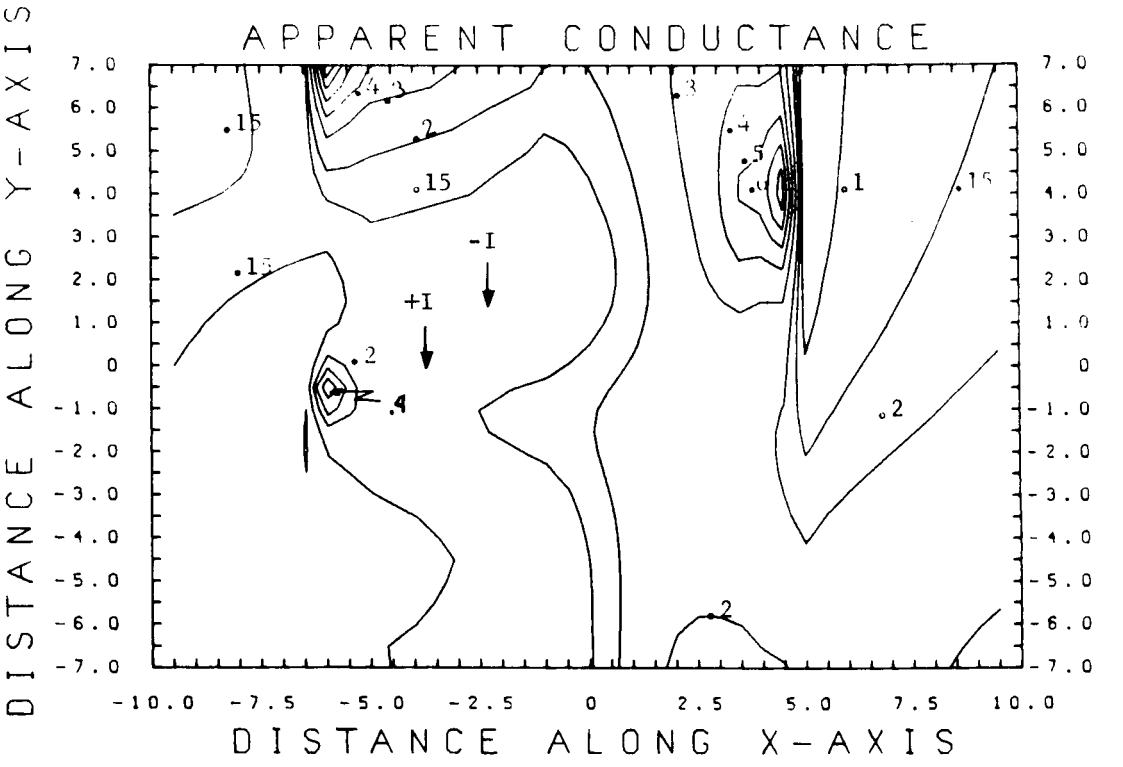
APPARENT CONDUCTANCE
DISTANCE ALONG Y-AXIS
DISTANCE ALONG X-AXIS
+I
-I
7.0
6.0
5.0
4.0
3.0
2.0
1.0
0
-1.0
-2.0
-3.0
-4.0
-5.0
-6.0
-7.0
-10.0
-7.5
-5.0
-2.5
2.5
5.0
7.5
10.0

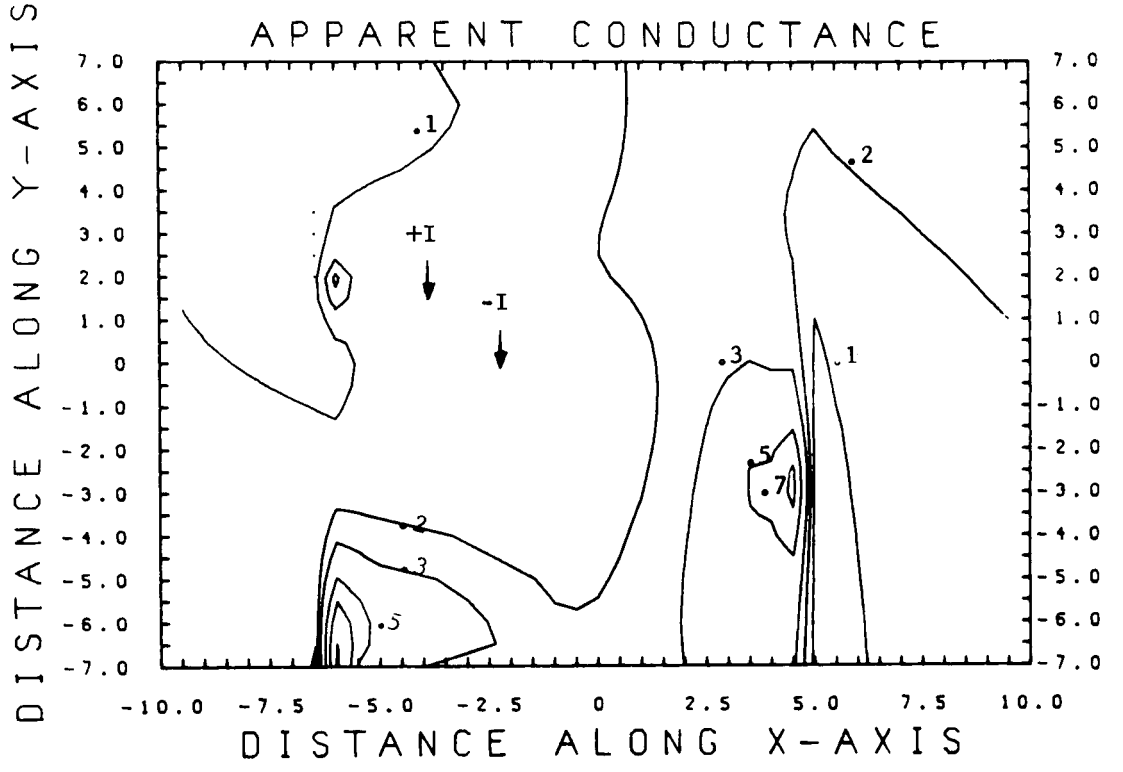
APPARENT CONDUCTANCE
DISTANCE ALONG Y-AXIS
DISTANCE ALONG X-AXIS
+I
-I
7.0
6.0
5.0
4.0
3.0
2.0
1.0
0
-1.0
-2.0
-3.0
-4.0
-5.0
-6.0
-7.0
-10.0
-7.5
-5.0
-2.5
2.5
5.0
7.5
10.0

Figure 31

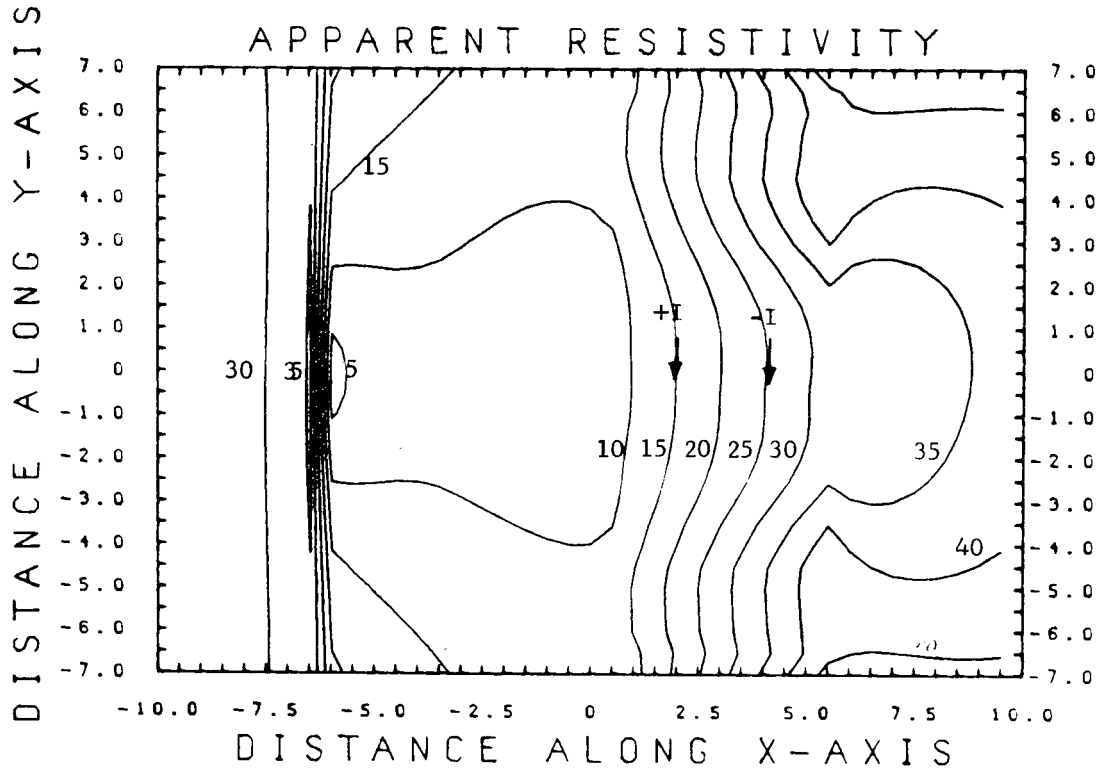
APPARENT RESISTIVITY
DISTANCE ALONG Y-AXIS
DISTANCE ALONG X-AXIS
+I
-I
15
30
35
5
10
15
20
25
30
35
40
7.0
6.0
5.0
4.0
3.0
2.0
1.0
0
-1.0
-2.0
-3.0
-4.0
-5.0
-6.0
-7.0
-10.0
-7.5
-5.0
-2.5
0
2.5
5.0
7.5
10.0

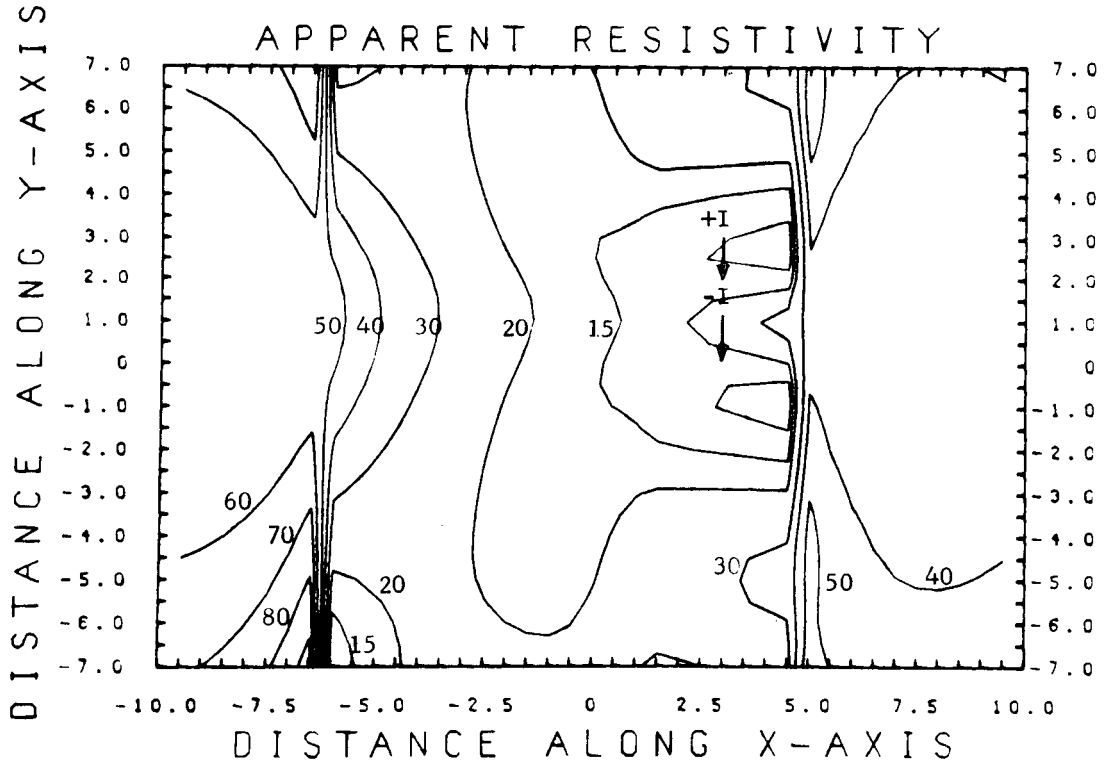
APPARENT RESISTIVITY
DISTANCE ALONG Y-AXIS
DISTANCE ALONG X-AXIS
+I
-I
50
40
30
20
15
60
70
80
20
15
30
50
40
7.0
6.0
5.0
4.0
3.0
2.0
1.0
0
-1.0
-2.0
-3.0
-4.0
-5.0
-6.0
-7.0
-10.0
-7.5
-5.0
-2.5
0
2.5
5.0
7.5
10.0

Figure 32

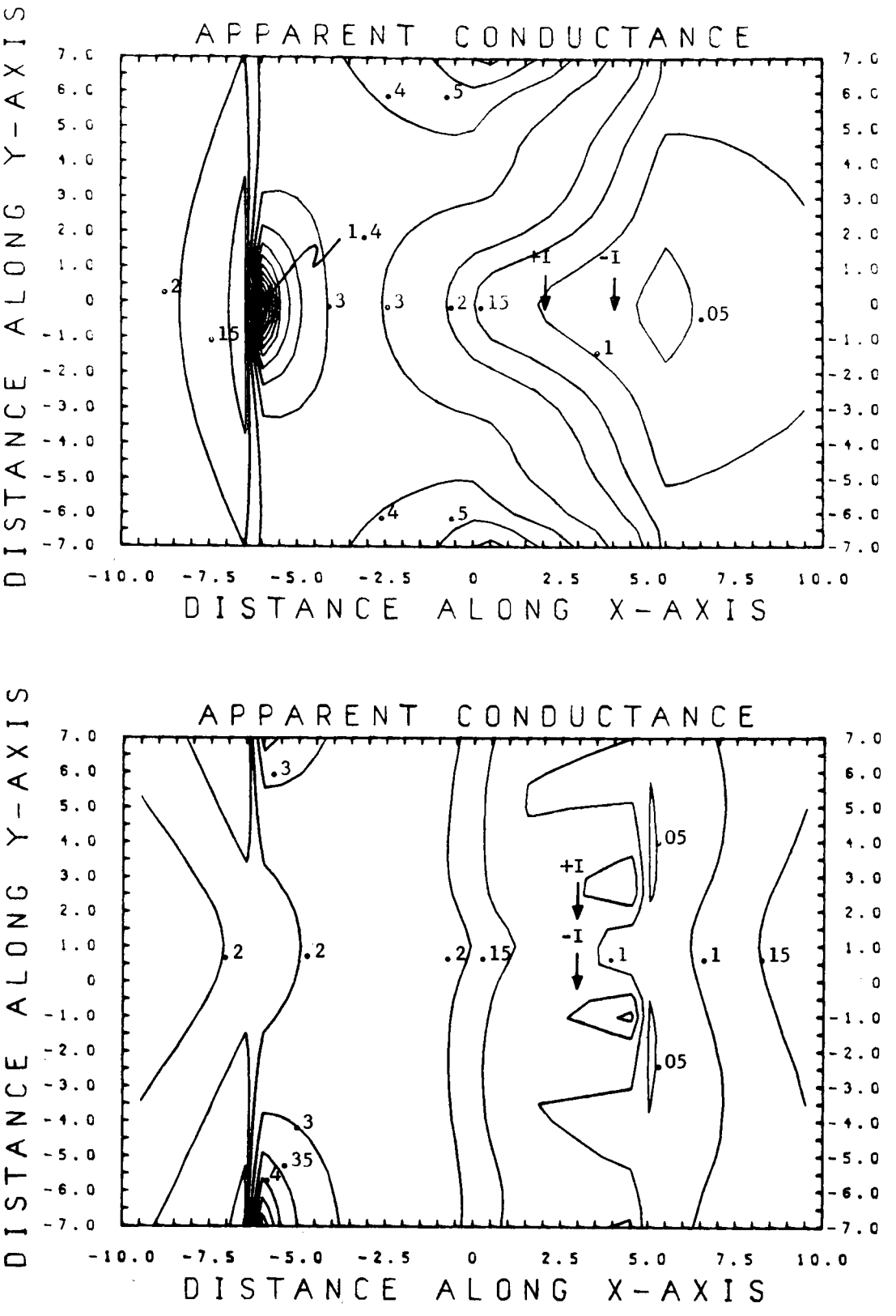
APPARENT CONDUCTANCE
DISTANCE ALONG Y-AXIS
DISTANCE ALONG X-AXIS
7.0
6.0
5.0
4.0
3.0
2.0
1.0
0
-1.0
-2.0
-3.0
-4.0
-5.0
-6.0
-7.0
-10.0
-7.5
-5.0
-2.5
2.5
5.0
7.5
10.0
.4
.5
1.4
.2
.3
.15
+I
-I
.05
.1
.35
APPARENT CONDUCTANCE
DISTANCE ALONG Y-AXIS
DISTANCE ALONG X-AXIS

Figure 33

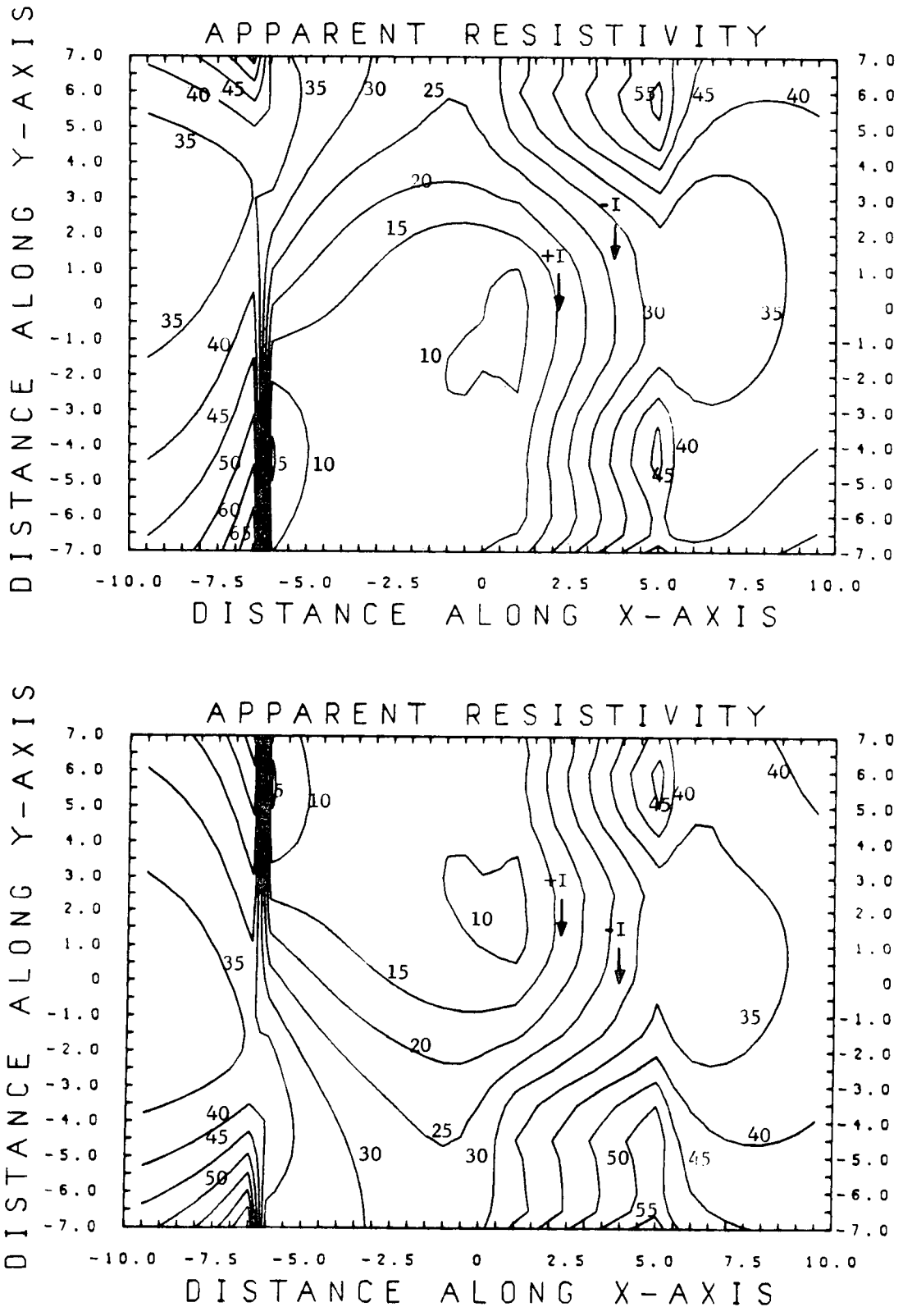
APPARENT RESISTIVITY
DISTANCE ALONG Y-AXIS
DISTANCE ALONG X-AXIS
7.0
6.0
5.0
4.0
3.0
2.0
1.0
0
-1.0
-2.0
-3.0
-4.0
-5.0
-6.0
-7.0
-10.0
-7.5
-5.0
-2.5
2.5
5.0
7.5
10.0
+I
-I
APPARENT RESISTIVITY
DISTANCE ALONG Y-AXIS
DISTANCE ALONG X-AXIS

Figure 34

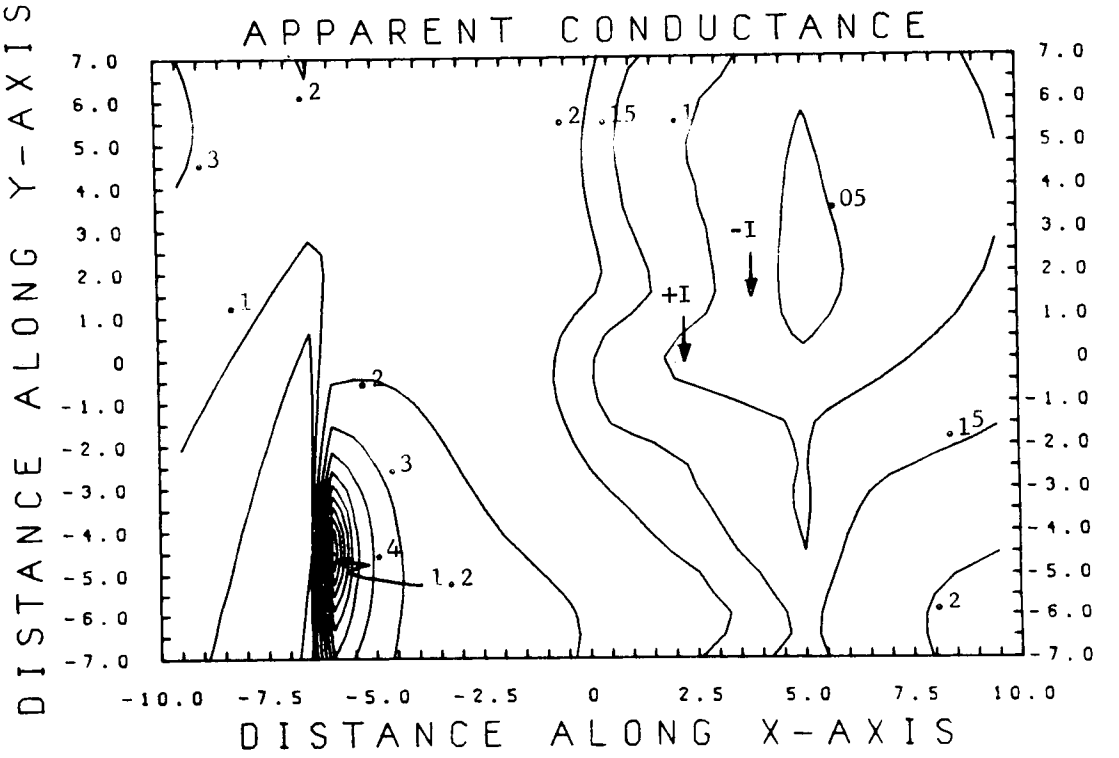
APPARENT CONDUCTANCE
DISTANCE ALONG Y-AXIS
DISTANCE ALONG X-AXIS
+I
-I
.3
.2
.2
.15
.1
.05
.1
.2
.3
.4
1.2
.15
.2
7.0
6.0
5.0
4.0
3.0
2.0
1.0
0
-1.0
-2.0
-3.0
-4.0
-5.0
-6.0
-7.0
-10.0
-7.5
-5.0
-2.5
0
2.5
5.0
7.5
10.0

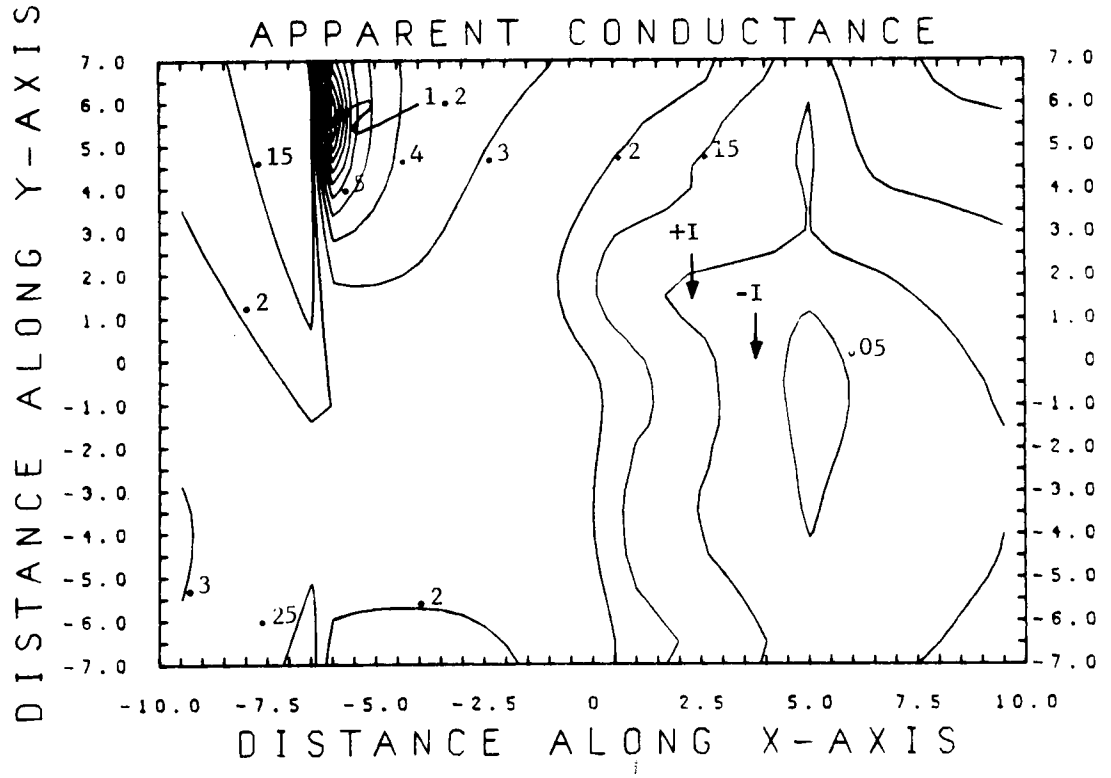
APPARENT CONDUCTANCE
DISTANCE ALONG Y-AXIS
DISTANCE ALONG X-AXIS
+I
-I
1.2
.15
.4
.3
.2
.15
.2
.05
.3
.25
.2
7.0
6.0
5.0
4.0
3.0
2.0
1.0
0
-1.0
-2.0
-3.0
-4.0
-5.0
-6.0
-7.0
-10.0
-7.5
-5.0
-2.5
0
2.5
5.0
7.5
10.0

Figure 35

TECHNICAL INFORMATION DEPARTMENT
LAWRENCE BERKELEY LABORATORY
UNIVERSITY OF CALIFORNIA
BERKELEY, CALIFORNIA 94720